frontiers in Marine Science

ORIGINAL RESEARCH
published: 19 August 2020
doi: 10.3389/fmars.2020.00665

Dragons of the Deep Sea: Kinorhyncha Communities in a Pockmark Field at Mozambique Channel, With the Description of Three New Species

Diego Cepeda[1], Fernando Pardos[1], Daniela Zeppilli[2] and Nuria Sánchez[2]*

[1] *Departamento de Biodiversidad, Ecología y Evolución, Facultad de Ciencias Biológicas, Universidad Complutense de Madrid, Madrid, Spain,* [2] *Laboratoire Environnement Profond, Institut Français de Recherche pour l'Exploitation de la Mer (IFREMER), Plouzané, France*

Cold seep areas are extremely reduced habitats with spatiotemporal variation of hydrocarbon-rich fluid seepage, low oxygen levels, and great habitat heterogeneity. Cold seeps can create circular to ellipsoid shallow depressions on the seafloor called pockmarks. We investigated two selected pockmarks, characterized by different gas emission, and two sites outside these geological structures at the Mozambique Channel to understand whether and how their environmental conditions affect the kinorhynch fauna in terms of density, richness, and community composition. A total of 11 species have been found living in the studied area, of which three are new species: *Fissuroderes cthulhu* sp. nov., *Fujuriphyes dagon* sp. nov., and *Fujuriphyes hydra* sp. nov. Densities outside the pockmarks are low and regularly decrease from the upper sediment layers, whereas inside the pockmarks, density reaches its highest value at layer 1–2 cm, strongly decreasing along the vertical profile from this depth. Areas under pockmark influence and locations outside pockmarks are similar in terms of species richness, but kinorhynchs showed a significant remarkable higher density at the pockmark sites. Additionally, species composition changes between habitats (inside and outside pockmarks) and between the two sampled pockmarks, with most of the species restricted to one of the studied habitats, except for *Condyloderes* sp. and *Echinoderes unispinosus* present both outside and inside the pockmarks. *Echinoderes hviidarum, E. unispinosus*, and *Fi. cthulhu* sp. nov., present at sites with gas emission, do not only survive under the specific pockmark conditions (characterized by hydrogen sulfide toxicity, methane high concentration, and low availability of dissolved oxygen) but even profit from a habitat with a likely lower competition for space and resources, flourishing and enhancing the density, most likely through the replacement with specialized species. Contrarily, species that only appear outside the pockmarks do not seem to cope with the presence of hydrogen sulfide and methane. Therefore, environmental factors linked to gas emissions have a major role driving the kinorhynch community composition.

Keywords: cold seeps, deep sea, ecology, kinorhynchs, meiofauna, diversity, taxonomy

OPEN ACCESS

Edited by:
Rui Rosa,
University of Lisbon, Portugal

Reviewed by:
Martin Vinther Sørensen,
University of Copenhagen, Denmark
Matteo Dal Zotto,
University of Modena and Reggio Emilia, Italy

****Correspondence:***
Diego Cepeda
diegocepeda@ucm.es

Specialty section:
This article was submitted to Global Change and the Future Ocean, a section of the journal Frontiers in Marine Science

Received: *30 November 2019*
Accepted: *21 July 2020*
Published: *19 August 2020*

Citation:
Cepeda D, Pardos F, Zeppilli D and Sánchez N (2020) Dragons of the Deep Sea: Kinorhyncha Communities in a Pockmark Field at Mozambique Channel, With the Description of Three New Species. Front. Mar. Sci. 7:665. doi: 10.3389/fmars.2020.00665

INTRODUCTION

Worldwide oceans cover about 361.9 million km^2 of the earth's surface, of which ∼70% are deep sea plains (Eakins and Sharman, 2010). Nowadays, ocean floor studies have experienced a strong revitalization, showing that the deep sea possesses prosperous, complex biological communities and a huge variety of geochemical environments that host unique species (Levin and Sibuet, 2012; Kennedy et al., 2019). Cold seeps are extreme, reduced habitats on the seafloor where hydrogen sulfide, methane, and other hydrocarbon-rich fluid seepage occurs (Kumar, 2017), causing a fall in oxygen levels and peaks of primary production due to chemoautotrophic organisms (Sibuet and Olu, 1998; Levin, 2005; Zeppilli et al., 2018). Cold seeps generate several geological structures such as pockmarks, circular to ellipsoid shallow depressions on the seafloor where the fluid emission varies spatiotemporally, cones (as mud volcanoes), carbonated structures, and brine pools, oval to rounded-shaped bodies of water that have a salinity higher than the surrounding ocean (Hovland and Judd, 1988; Dando et al., 1991).

Organisms inhabiting cold seeps take advantage of the habitat heterogeneity formed by the variable fluid release intensity and the hydrocarbon-rich fluid concentration of the sediment to occupy extreme, reduced niches that other organisms are unable to inhabit (Levin, 2005; Guillon et al., 2017). These adapted species can reach high levels of abundance and biomass (Rouse and Fauchald, 1997; Levin, 2005; Seitzinger et al., 2010; Vanreusel et al., 2010; Guillon et al., 2017; Sun et al., 2017) as a consequence of few species having evolved the morpho-physiological adaptations required to live in such a challenging habitat (Hourdez and Lallier, 2006; Zeppilli et al., 2018).

Studies of Kinorhyncha from the deep sea have frequently reported unidentified species, mostly from the Indian, Pacific, and Atlantic Oceans (Neuhaus, 2013; Zeppilli et al., 2018). More recently, studies to the species level have received a strong boost, and up to 45 species have recently been described or reported from this environment (Neuhaus and Blasche, 2006; Sørensen, 2008a; Neuhaus and Sørensen, 2013; Sánchez et al., 2014a,b, 2019a; Adrianov and Maiorova, 2015, 2016, 2018a,b; Grzelak and Sørensen, 2018, 2019; Sørensen and Grzelak, 2018; Sørensen et al., 2018, 2019; Yamasaki et al., 2018a,b,c, 2019; Cepeda et al., 2019a). Of these, some species seem to possess wider ranges of distribution than their congeners from the coastal zone. For instance, *Condyloderes kurilensis* Adrianov and Maiorova (2016), and *Fissuroderes higginsi* Neuhaus and Blasche (2006), were originally described from the Kuril-Kamchatka Trench (northwestern Pacific) and New Zealand (southwestern Pacific), respectively, and later found in the deep-sea waters off Oregon and California (northeastern Pacific) and the Clarion-Clipperton Zone (Neuhaus and Blasche, 2006; Adrianov and Maiorova, 2016; Sørensen et al., 2018; Sánchez et al., 2019a). More striking are the cases of *Campyloderes vanhoeffeni* Zelinka, 1913, distributed worldwide in both coastal waters and deep sea (Neuhaus and Sørensen, 2013) and *Echinoderes unispinosus* present in the deep sea of the Atlantic and the Pacific Oceans (Sørensen et al., 2018; Yamasaki et al., 2019; Álvarez-Castillo et al., 2020). This apparent cosmopolitanism might suggest that the deep sea environmental homogeneity promotes much wider distributional ranges than those observed from shallow water species (Sørensen et al., 2018). However, the possibility of having complexes of cryptic species must also be taken into account, since speciation in deep sea environments is not always accompanied by conspicuous morphological changes (Janssen et al., 2015).

Despite these hypotheses, little is known about the main environmental factors that shape the kinorhynch communities in general and particularly in deep sea, extreme environments. Some recent studies performed in the Arctic Ocean and the Gulf of Mexico determined that sediment grain size and trace metals are the variables that most seem to affect the Kinorhyncha species composition (Landers et al., 2018; Grzelak and Sørensen, 2019). Additionally, Álvarez-Castillo et al. (2015) concluded that kinorhynchs are somehow affected by pore water pH in reduced environments such as CO_2 vents. Also, kinorhynch densities have been proven to vary with the sulfide and organic matter concentrations of the seafloor (Sutherland et al., 2007; Mirto et al., 2012; Dal Zotto et al., 2016; Landers et al., 2020). In this context, the main aim of the present paper is to characterize the kinorhynch community associated with pockmarks in the Mozambique Channel deep sea to (1) identify and describe the new species inhabiting the area, (2) report potential kinorhynch species as indicators of cold seep areas, and (3) determine possible differences in richness, density, and species composition inside and outside pockmarks and along the vertical profile.

MATERIALS AND METHODS

Study Area, Sampling, and Processing

A pockmark cluster area was selected for the present study in the deep sea Mozambique Channel, off Mozambique and Madagascar (western Indian Ocean). Samples were collected during the *PAMELA-MOZ01* and *PAMELA-MOZ04* campaigns aboard the R/V *L'Atalante* and *Pourquoi pas?* (Genavir-Ifremer), respectively (Olu, 2014; Jouet and Deville, 2015). Multibeam echosounders and seabed inspection with a deep-towed camera Scampi were used to detect the location of pockmarks obtaining bathymetric data and identifying cold seep macrofauna indicators. Two active pockmarks and two sites outside any pockmark were selected.

MOZ04_MTB2: S 15 21.685; E 45 57.378; 754 m.
MOZ01_MTB3: S 15°21.695; E 45°57.388; 757 m.
MOZ04_MTB1: S 15°21.812; E 45°57.628; 735 m.
MOZ01_MTB6: S 15°31.148; E 45°42.931; 789 m depth.

Samples were obtained with a Barnett-type multi-corer (MTB) with three cores by deployment. Each core of 6.2 cm inner diameter (total surface area of 30.2 cm^2) was horizontally sliced into five layers: layer 1 (0–1 cm depth), layer 2 (1–2 cm depth), layer 3 (2–3 cm depth), layer 4 (3–4 cm depth), and layer 5 (4–5 cm depth). Each subsample was fixed in 4% formalin. Subsequently, the sediment of each slice was sieved on 1-mm and 32-μm sieves at the Ghent laboratory (Belgium) and the IFREMER laboratory (France), and the metazoan meiofauna was separated from the sediment by Ludox centrifugation (Heip et al., 1985) and subsequently fixed in 4% formalin.

Species Identification and Description

Kinorhynchs were separated from the remaining meiofauna using an Irwin loop and washed with distilled water to remove formalin remnants. Kinorhynchs were mounted and identified to species level, except for the juveniles that could be identified only to class level.

For light microscopy (LM), specimens were dehydrated through a graded series of 25, 50, 75, and 100% glycerine to be mounted on glass slides with Fluoromount G®. The mounted specimens were studied, identified, and photographed with a Leica DM2500® LED compound microscope equipped with differential interference contrast (DIC).

For scanning electron microscopy (SEM), specimens were sonically cleaned and transferred to 70% ethanol and progressively dehydrated through a graded series of 80, 90, 95, and 100% ethanol. Hexamethyldisilazane (HMDS) was used for chemical drying through a HMDS-ethanol series. Specimens were coated with gold and mounted on aluminum stubs to be examined with a JSM 6335-F JEOL SEM at the "ICTS Centro Nacional de Microscopía Electrónica" (Universidad Complutense de Madrid, Spain). For species descriptions, line art and image plates composition were done using Adobe Photoshop and Illustrator CC-2014 software. Type and additional material were deposited at the Natural History Museum of Denmark (NHMD).

Environment Characterization

To test the influence of the environment over the kinorhynch communities and detect potential species as indicators of seepages, we selected hydrogen sulfide (H_2S) and methane (CH_4) as a proxy of cold seep activity.

H_2S concentration was quantified by colorimetry (Fonselius, 1983) after precipitation of the sulfide with zinc chloride on board. The concentration was detected in a high level only at the pockmark site MOZ04-MTB1. CH_4 was determined by gas chromatography headspace technique (GC/HSS) (Sarradin and Caprais, 1996), following different sampling techniques between the two cruises. In MOZ-01, 5 ml of pore waters was collected in 10-ml vials by Rhizon samplers (Rhizosphere Research Products R.V., Wageningen), which are thin rods covered by hydrophilic porous polymer designed to extract water from sediment using a vacuum (Seeberg-Elverfeldt et al., 2005); then, 20 μl of a saturated mercuric hydrochloride solution was added to preserve samples. In MOZ-04, 3 ml of sediment was collected in 20-ml vials, where 5 ml of a solution of sodium hydroxide at 1 M was added to avoid any bacterial activity. CH_4 was found at the two study pockmarks. The methodology followed during the cruise MOZ01, using Rhizon samplers, induced a degassing step of dissolved methane in the pore waters, while methane is more preserved by collecting directly the sediment, as done during the cruise MOZ04.

Data Processing and Statistical Analyses

The effect of the environmental conditions on kinorhynch community structure and assemblage was assessed using three community descriptors as response variables: (1) richness, (2) density, and (3) species composition. Richness was measured as number of species, and density as number of individuals per 10 cm^2, including both adults and juveniles.

Kruskal–Wallis analyses (KW) were conducted through R v.6.3.1 software to test differences in kinorhynch richness and density. We assessed changes in community structure through different approaches: along the vertical profile of each habitat (inside and outside pockmarks, considering five layers: 0–1, 1–2, 2–3, 3–4, and 4–5 cm), between habitats (inside vs. outside pockmarks), and between sites sampled at the same habitat.

Differences in adult community composition between habitats and between sites of the same habitat were tested by permutational multivariate analysis of variance (PERMANOVA) calculated with the function "adonis" in the R package *vegan* v. 2.2-1 (Oksanen et al., 2018). Distance matrices were calculated using both Jaccard (incidence) and Ružièka [abundance transformed to $\log_{10}$(abundance + 1)] dissimilarity indices through the function "beta" of the R package *vegan* v. 2.2-1 (Oksanen et al., 2015). In order to further investigate the environmental factors that drive the community composition, H_2S was used as categorical covariate variable (two levels: absence, all layers with concentration of 0 μM; high, layers with concentrations > 200 Mm). CH_4 was detected at both pockmark sites (MOZ01-MTB06 and MOZ04-MTB1), but the concentration was measured following different methods and therefore data cannot be truly comparable. We conducted a principal component analysis (PCA) in abundance using the function "rda" of the R package *vegan* v. 2.2-1 (Oksanen et al., 2015) to visualize community composition variations among sites. Abundance data were transformed in order to use the Hellinger distance among samples using the function "decostand" of the R package *vegan* 2.4-4 (Oksanen et al., 2018), since double absence is not considered as an indicator of similarity and it gives a lower weight to dominant species (Legendre and Gallagher, 2001). A *post hoc* explaining of the PCA axes by adding environmental variables was performed by the function "envfit" of the R package *vegan* 2.4-4 (Oksanen et al., 2018).

RESULTS

Taxonomic Account

Class Allomalorhagida Sørensen et al., 2015.

Family Pycnophyidae Zelinka, 1896.

Genus *Fujuriphyes* Sánchez et al., 2016.

Fujuriphyes dagon sp. nov.

urn:lsid:zoobank.org:act:28C303EF-46AE-4304-887C-9202B7386AB9 (**Figures 1–4**).

Material examined

Holotype, adult female, collected in October 2014 at Mahavavy area, Mozambique Channel, western Indian Ocean (−15° 32.532′, 45° 42.894′) at 775 m depth; mounted in Fluoromount G®, deposited at NHMD under accession number: 669762. Paratypes, three adult males, with same collecting data as

holotype; mounted in Fluoromount G®, deposited at NHMD under accession numbers: 669763–669765. Two additional specimens mounted for SEM, same collecting data as type material, deposited at the Meiofauna Collection of the UCM.

Diagnosis

Fujuriphyes without middorsal processes or elevations. Unpaired paradorsal setae on segments 2, 4, 6, and 8. Laterodorsal setae on segments 2–10. Lateroventral setae on even segments. One pair of ventrolateral setae on segments 2–4 and 6–9, and two pairs on segment 5. Males with ventromedial tubes on segment 2. Lateral terminal spines present.

Etymology

The species is named after the fictional deity Dagon (also known as Father Dagon), created by the American writer of horror fiction H.P. Lovecraft (1890–1937) and firstly introduced in the short story "Dagon," published in 1919. In the pantheon of Lovecraftian cosmic entities, Dagon presides over the Deep Ones, an amphibious humanoid race indigenous to Earth's oceans.

Description

See **Supplementary Table 1.1** for measurements and dimensions and **Supplementary Table 1.2** for summary of seta, spine, tube, glandular cell outlet, and sensory spot locations.

Ring 00 of mouth cone with nine equally sized outer oral styles (**Figure 2**) composed of a single, flexible unit, wider at the base, which bears a fringed sheath, progressively tapering toward a distal, pointed tip. Outer oral styles located anterior to each introvert sector, except in the middorsal section 6 where a style is missing (**Figure 2**).

Introvert with six transverse rings of scalids and 10 longitudinal sectors defined by the arrangement of the primary spinoscalids (**Figures 2**, **3H**). Ring 01 with 10 primary spinoscalids, larger than remaining ones, each one composed of a basal, rectangular, wide sheath and a distal, elongated, flexible, distally pointed end piece (**Figures 2**, **3H**). Ring 02 with 10 regular-sized scalids, arranged as one medially in each sector (**Figure 2**). Scalids of this and the following rings are morphologically similar to the primary spinoscalids but smaller (**Figure 3H**). Ring 03 with 20 regular-sized scalids, arranged as 2 in each sector (**Figures 2**, **3H**). Ring 04 with 5 regular-sized scalids, arranged as 1 medially in each odd-numbered sector (**Figures 2**, **3H**). Ring 05 with 15 regular-sized scalids, arranged as 1 medially in each even-numbered sector and 2 in each odd-numbered sector (**Figure 2**). Ring 06 also with 15 regular-sized scalids, arranged as 2 in each even-numbered sector and 1 medially in each odd-numbered sector (**Figure 2**). The location of scalids in rings 01–06 follows a strict pattern around the introvert: each even-numbered sector carries six regular-sized scalids as two chevrons, whereas each odd-numbered sector bears seven regular-sized scalids as a double diamond (**Figures 2**, **3H**).

Neck with four dorsal and two ventral sclerotized placids (**Figures 1A–C**). Dorsal placids rectangular, wide, mesial ones broader (ca. 30–32 μm wide at the base) than lateral ones (ca. 20–23 μm wide at the base), with a notch in the middle region (**Figure 1B**). Ventral placids (ca. 29–31 μm wide at the base) more quadrangular than dorsal ones, with the posterolateral margins curved toward the sternal plates of the first trunk segment (**Figures 1A,C**). A ring of 14 trichoscalids posterior to the scalid rings, arranged as 2 in the odd-numbered sectors (except sector 1 with a single trichoscalid) and 1 in the even-numbered sectors of the introvert (**Figures 2**, **3H**).

Trunk rectangular, stout, triangular in cross-section, composed of 11 segments (**Figures 1A,B**, **3A**, **4A**). Segment 1 with one tergal, two episternal, and one midsternal plate (**Figures 1A–C**, **3A–C**); remaining segments with one tergal and two sternal plates (**Figures 1A–D**, **3A**). Maximum sternal width at segment 6, almost constant throughout the trunk, progressively tapering at the last trunk segments (**Figures 1A,B**, **3A**, **4A**). Sternal cuticular plates relatively narrow in the ratio of maximum sternal width to trunk length (MSW-6:TL interval ratio = 21.9–24.9), giving the animal a slender appearance (**Figures 1A,B**, **3A**, **4A**). Segments 1–10 with oval glandular cell outlets in subdorsal and ventromedial positions (**Figures 1A–C**, **3B–G,I,J**). Segments 2–10 with paired cuticular ridges in laterodorsal and ventrolateral positions, the latter with adjacent, minute glandular cell outlets (**Figures 1A–D**, **3A–G,I,J**). Cuticular hairs acicular, densely covering the cuticular surface of segments 2–10 from paralateral to ventromedial positions (**Figures 4D–G, H–K**). Muscular scars very conspicuous in laterodorsal and ventromedial positions (**Figures 1A–D**, **3B–G,I,J**). Areas with superficially wrinkled cuticle present in ventrolateral position on segments 2–10 and paralateral position on segment 1 (**Figures 1A,C**). Pachycycli and ball-and-socket joints well-developed and thick on segments 2–10 (**Figures 1A–D**, **3A**). Apodemes present on segments 8–10 (**Figures 1A**, **3A**). Posterior margin of segments straight, showing primary pectinate fringes with weakly serrated free flaps; secondary pectinate fringes also straight and finely serrated (**Figures 1A–D**).

Segment 1 without middorsal cuticular process or elevation. Anterolateral margins of the tergal plate as horn-like, distally rounded extensions (**Figures 1A–C**, **3A**, **4A,B**). Anterior margin of tergal plate smooth, followed by a crenulated area (**Figures 1B**, **3B**, **4A,B**). Anterior margin of sternal plates with a wavy median ridge of cuticle (**Figures 1A,C**, **3C**). Midsternal plate trapezoidal, laterally extended at its base, with a lateral constriction near its anterior margin and a straight posterior margin (**Figures 1A,C**, **3C**). Sensory spots in subdorsal (two pairs), laterodorsal (one pair), ventrolateral (two pairs), and ventromedial (one pair) positions (**Figures 1A–C**, **3B,C**, **4B,C**).

Segment 2 without middorsal process or elevation. Unpaired seta in paradorsal position; paired setae in laterodorsal, lateroventral, and ventrolateral positions (**Figures 1A–C**, **3D,E**, **4H,I**). Sensory spots in subdorsal (one pair), laterodorsal (one pair), and ventromedial (two pairs) positions (**Figures 1A–C**, **3D,E**, **4H,I**). Males with sexually dimorphic tubes in ventromedial position (**Figures 1C**, **4I**).

Segment 3 without middorsal process or elevation. Paired setae in laterodorsal and ventrolateral positions (**Figures 1A,B**, **3D,E**). Sensory spots in subdorsal (one pair), laterodorsal (one pair), and ventromedial (two pairs) positions (**Figures 1A,B**, **3D,E**).

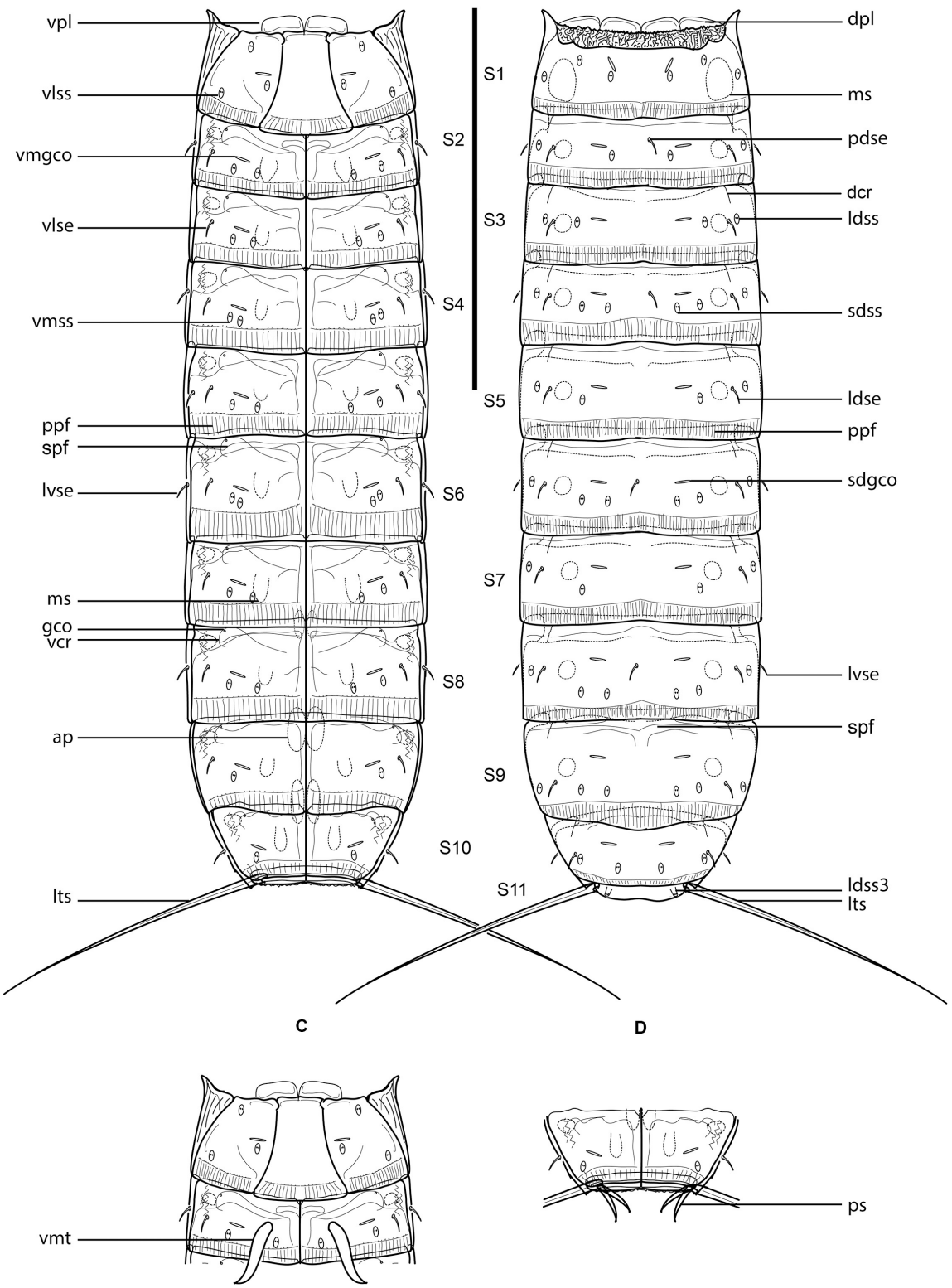

FIGURE 1 | Continued

FIGURE 1 | Line art illustrations of *Fujuriphyes dagon* sp. nov. **(A)** Female, ventral view; **(B)** female, dorsal view; **(C)** male, segments 1–2, ventral view; **(D)** male, segments 10–11, ventral view. Scale bar: 250 μm. Abbreviations: ap, apodeme; dcr, dorsal cuticular ridge; dpl, dorsal placid; gco, glandular cell outlet; ldse, laterodorsal seta; ldss, laterodorsal sensory spot; ldss3, laterodorsal type 3 sensory spot; lts, lateral terminal spine; lvse, lateroventral seta; ms, muscular scar; pdse, paradorsal seta; ppf, primary pectinate fringe; ps, penile spine; sdgco, subdorsal glandular cell outlet; sdss, subdorsal sensory spot; spf, secondary pectinate fringe; vcr, ventral cuticular ridge; vlse, ventrolateral seta; vlss, ventrolateral sensory spot; vmgco, ventromedial glandular cell outlet; vmss, ventromedial sensory spot; vmt, ventromedial tube; vpl, ventral placid.

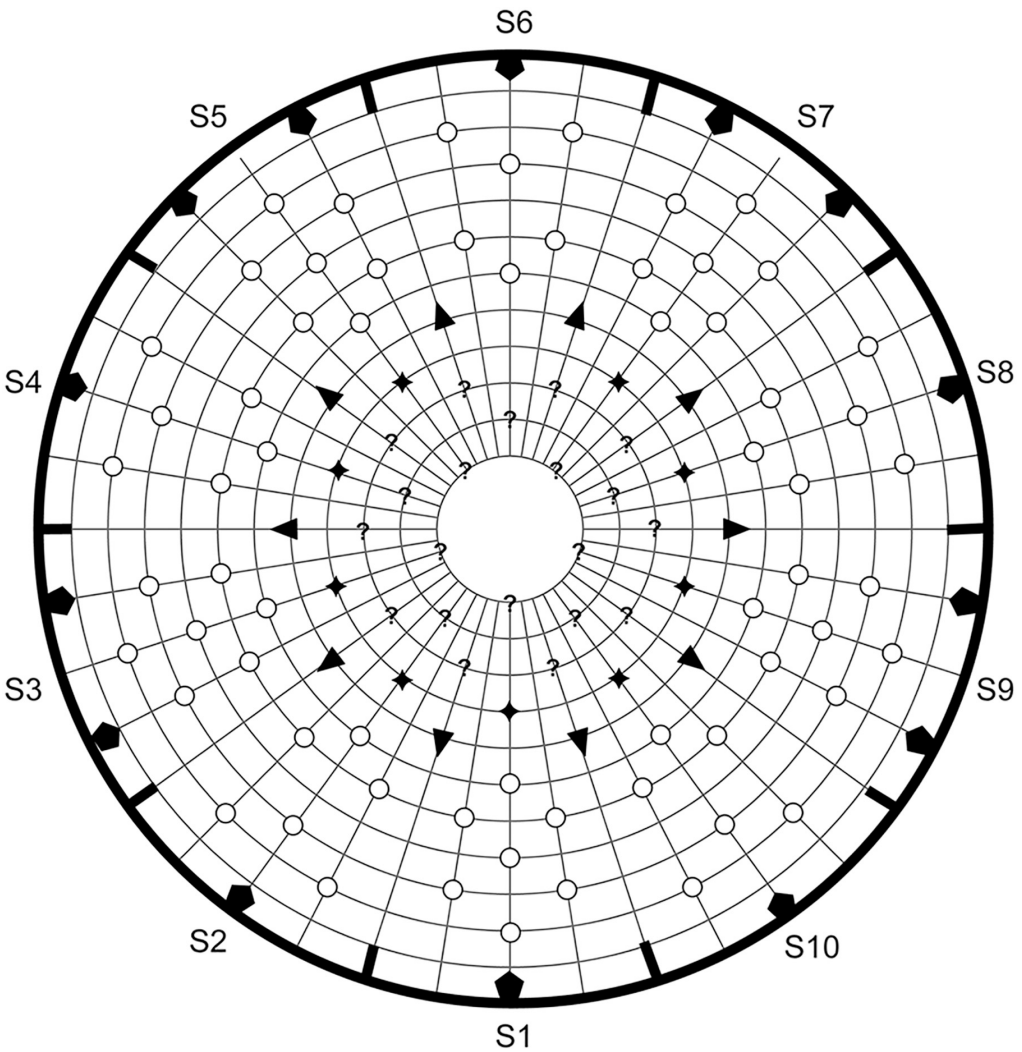

FIGURE 2 | Diagram of mouth cone, introvert, and trichoscalids in *Fujuriphyes dagon* sp. nov., with indication of oral style, scalid, and trichoscalid arrangement.

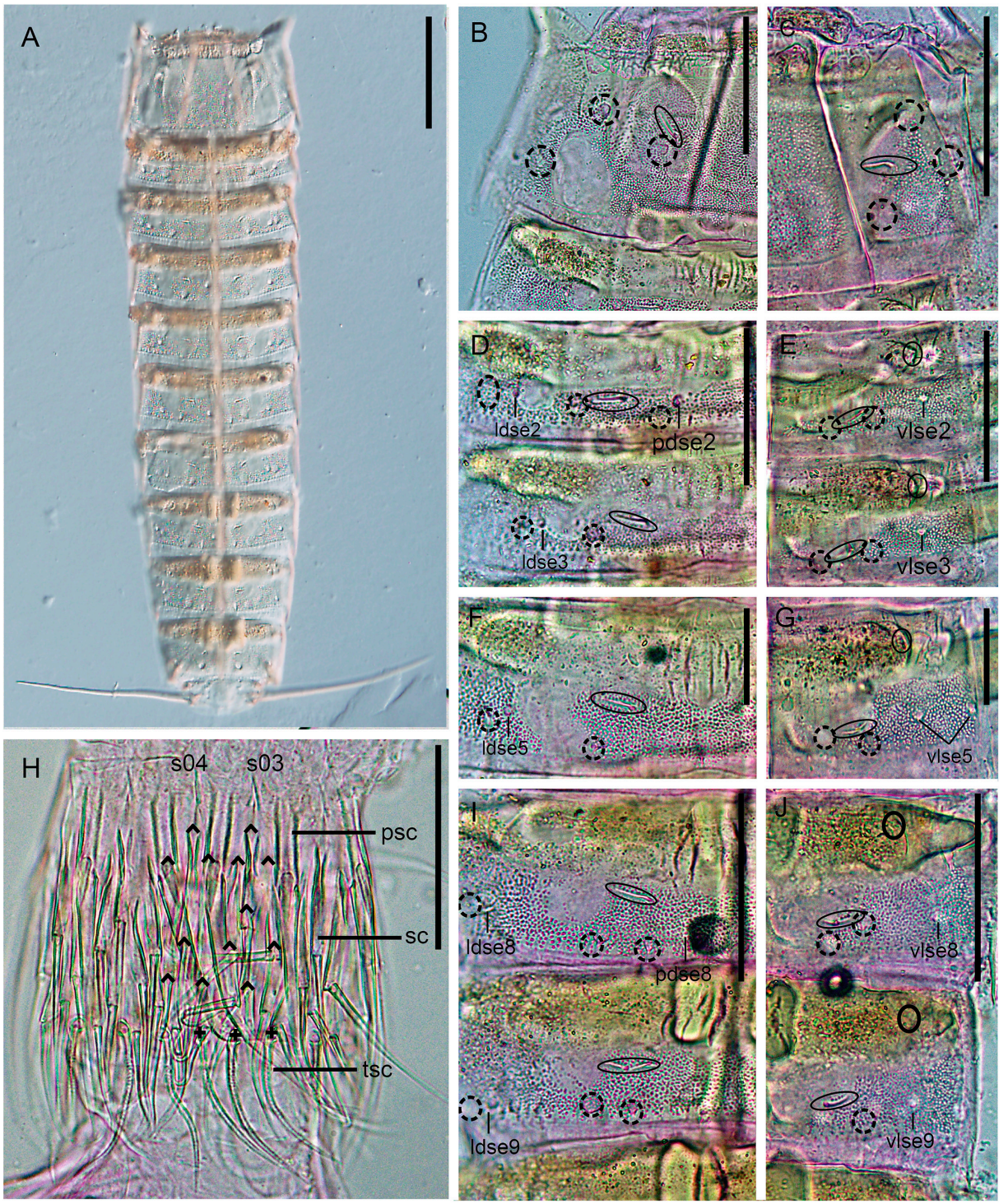

FIGURE 3 | Light micrographs showing trunk overview and details in the head and main trunk cuticular characters of female holotype NHMD 669762 **(B–J)** and male paratype NHMD 669763 **(A)** of *Fujuriphyes dagon* sp. nov. **(A)** Dorsal overview of trunk; **(B)** middorsal to paralateral view on right half of tergal plate of segment 1; **(C)** ventrolateral to ventromedial view on left half of sternal plates of segment 1; **(D)** middorsal to laterodorsal view on right half of tergal plate of segments 2–3; **(E)** left sternal plates of segments 2–3; **(F)** middorsal to laterodorsal view on right half of tergal plate of segment 5; **(G)** left sternal plate of segment 5; **(H)** introvert, with detail of primary spinoscalid, regular-sized scalid, and trichoscalid arrangement of sectors 03–04; **(I)** middorsal to laterodorsal view on right half of tergal plate of segments 8–9; **(J)** left sternal plates of segments 8–9. Scale bars **(A):** 250 μm; **(B–E, H–J)**: 62 μm; **(F)** and **(G):** 31 μm. Abbreviations: ldse, laterodorsal seta; pdse, paradorsal seta; psc, primary spinoscalid; s, sector of introvert; sc, regular-sized scalid; tsc, trichoscalid; vlse, ventrolateral seta; numbers after abbreviations indicate corresponding segment or sector of introvert; carets indicate the arrangement of scalids, and crosses that of trichoscalids; sensory spots are marked as dashed circles, and glandular cell outlets as continuous circles.

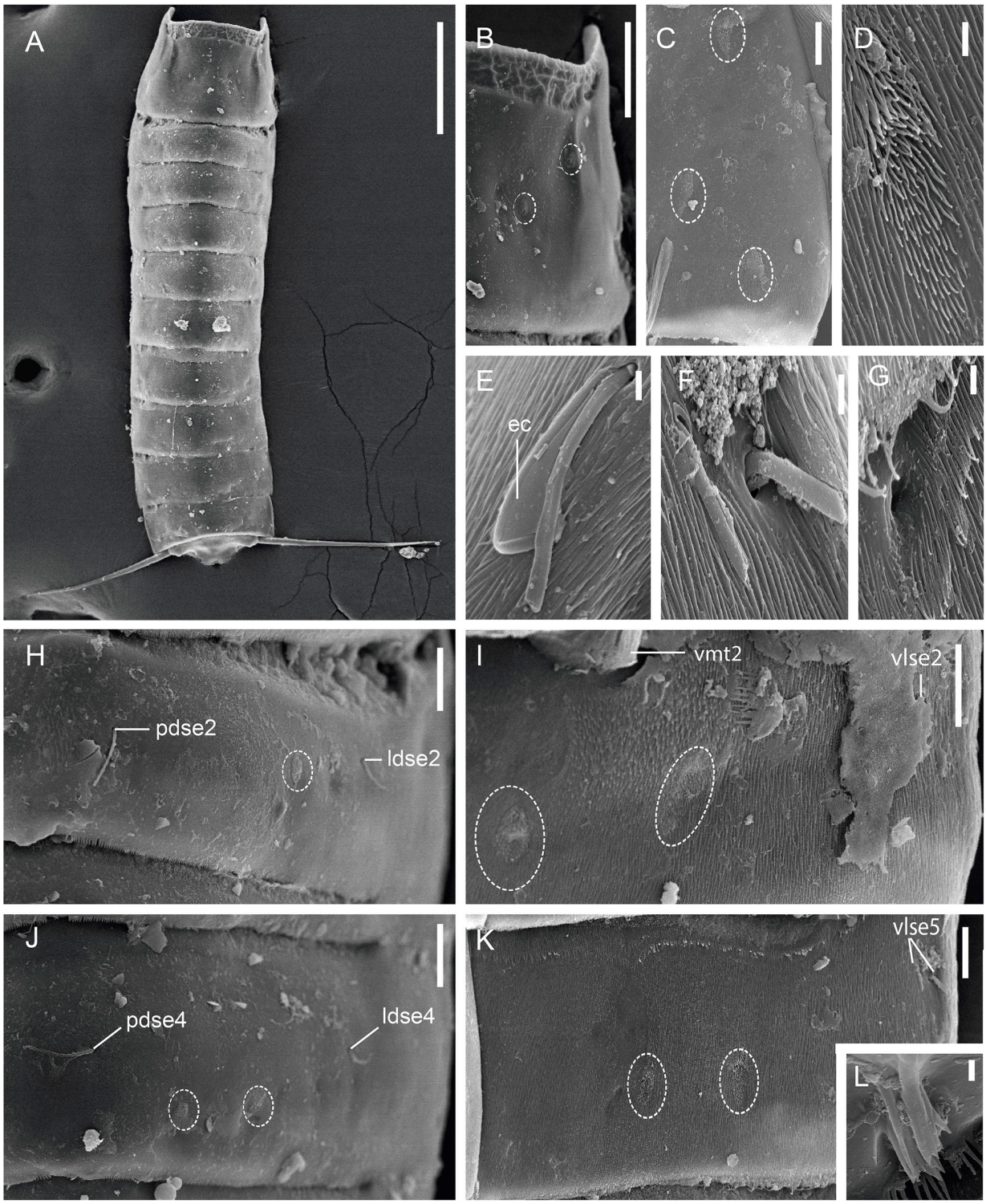

FIGURE 4 | Scanning electron micrographs showing trunk overview and details in the main trunk cuticular appendages of a male of *Fujuriphyes dagon* sp. nov. **(A)** Dorsal overview of trunk; **(B)** middorsal to subdorsal view on left half of tergal plate of segment 1; **(C)** left episternal plate of segment 1; **(D)** ventromedial sensory spot of segment 5; **(E)** lateroventral seta of segment 10; **(F)** ventrolateral setae of segment 5; **(G)** ventral cuticular ridge and associated glandular cell outlet of segment 6; **(H)** middorsal to laterodorsal view on left half of tergal plate of segment 2; **(I)** left sternal plate of segment 2; **(J)** middorsal to laterodorsal view on left half of tergal plate of segment 4; **(K)** left sternal plate of segment 5; **(L)** laterodorsal type 3 sensory spot of segment 11. Scale bars: **(A):** 300 μm; **(B):** 30 μm; **(C,E,H–L)**: 10 μm; **(D,F,G):** 1 μm. Abbreviations: ec, epibiontic Ciliophora; ldse, laterodorsal seta; pdse, paradorsal seta; vlse, ventrolateral seta; vmt, ventromedial tube; numbers after abbreviations indicate corresponding segment; sensory spots are marked as dashed circles.

Segment 4 without middorsal process or elevation. Unpaired seta in paradorsal position; paired setae in laterodorsal, lateroventral, and ventrolateral positions (**Figures 1A,B**, **4J**). Sensory spots in subdorsal (two pairs), laterodorsal (one pair), and ventromedial (two pairs) positions, with the more mesial ventromedial pair laterally shifted compared to those of previous segments (**Figures 1A,B**, **4J**).

Segment 5 without middorsal process or elevation. Two pairs of setae in ventrolateral position; one pair in laterodorsal position (**Figures 1A,B**, **3F,G**, **4F,K**). Sensory spots in subdorsal (one pair), laterodorsal (one pair), and ventromedial (two pairs) positions, the latter aligned with those of segment 3 (**Figures 1A,B**, **3F,G**, **4D,K**).

Segment 6 similar to segment 4 in the arrangement of setae and sensory spots (**Figures 1A,B**, **4G**).

Segment 7 similar to segment 3 in the arrangement of setae and sensory spots (**Figures 1A,B**).

Segment 8 without middorsal process or elevation. Unpaired seta in paradorsal position; paired setae in laterodorsal, lateroventral, and ventrolateral positions (**Figures 1A,B**, **3I,J**). Sensory spots in subdorsal (two pairs), laterodorsal (one pair), and ventromedial (two pairs) positions, the latter aligned with those of the previous segment (**Figures 1A,B**, **3I,J**).

Segment 9 without middorsal process or elevation. Paired setae in laterodorsal and ventrolateral positions (**Figures 1A,B**, **3I,J**). Sensory spots in subdorsal (two pairs), laterodorsal (one pair), and ventromedial (one pair) positions (**Figures 1A,B, 3I,J**). Nephridiopores not observed.

Segment 10 without middorsal process or elevation. Paired setae in laterodorsal and lateroventral positions (**Figures 1A,B,D**, **4E**). One pair of sensory spots in subdorsal, laterodorsal, and ventromedial positions (**Figures 1A,B,D**).

Segment 11 with one pair of type 3 sensory spots in laterodorsal position (**Figures 1B**, **4L**). Males with two pairs of sexually dimorphic penile spines and genital pores (**Figure 1D**). Lateral terminal spines long (LTS:TL interval ratio = 30.1–31.9), robust, widely spread, apparently rigid (**Figures 1A,B**, **3A**, **4A**).

Associated kinorhynch fauna

Fujuriphyes dagon sp. nov. co-occurred with *Condyloderes* sp., *E. unispinosus* and *Fissuroderes cthulhu* sp. nov. in the analyzed samples.

Fujuriphyes hydra sp. nov.

urn:lsid:zoobank.org:act:28E6A464-9534-46AC-A113-16492D6E52BE (**Figures 5**, **6**).

Material examined

Holotype, adult female, collected in November 2015 at Betsiboka area, Mozambique Channel, western Indian Ocean (−15° 21.685′, 45° 57.392′) at 754 m depth; mounted in Fluoromount G®, deposited at NHMD under accession number: 669766. Paratypes, two adult males and one adult female, with same collecting data as holotype; mounted in Fluoromount G®, deposited at NHMD under accession numbers: 669767–669769.

Diagnosis

Fujuriphyes with middorsal elevations on segments 1–10, with the elevation of segment 10 appearing smaller and thinner than the others. Unpaired paradorsal setae on segments 2, 4, and 6, and paired on segment 8. Paralateral setae on segment 1. Laterodorsal setae on segments 2–9. One pair of lateroventral setae on segments 2, 4, 6, and 8, and two pairs on segment 10. One pair of ventrolateral setae on segments 3–4 and 6–8, and two pairs on segment 5. Ventromedial setae on segments 2 (only females) and 9. Males with ventromedial tubes on segment 2. Lateral terminal spines present.

Etymology

The species is named after the fictional deity Hydra (also known as Mother Hydra), created by the American writer of cosmic horror fiction H.P. Lovecraft (1890–1937) and firstly introduced in the short story "The Shadow over Innsmouth," published in 1936. In the pantheon of Lovecraftian cosmic entities, Mother Hydra is the consort of Father Dagon.

Description

See **Supplementary Table 1.3** for measurements and dimensions, and **Supplementary Table 1.4** for summary of cuticular elevation, seta, spine, tube, glandular cell outlet, and sensory spot locations.

The analyzed specimens were not suitable for head examinations; hence, data on morphology, number, and arrangement of scalids and oral styles are not available.

Neck with four dorsal and two ventral, slightly sclerotized placids (**Figures 5A–C**). Dorsal placids rectangular, wide, longitudinally compressed; mesial ones broader (ca. 25–26 μm wide at the base), with the margins closest to the lateral ones more elevated; lateral ones narrower (ca. 20–21 μm wide at the base), with the margins closest to the mesial ones more elevated (**Figure 5B**). Ventral placids also rectangular but much more elongated (ca. 37–40 μm wide at the base), getting narrower toward the lateral sides (**Figures 5A,C**).

Trunk rectangular, stout, strongly sclerotized, triangular in cross-section, composed of 11 segments (**Figures 5A,B**, **6A**). Segment 1 with one tergal, two episternal, and one midsternal plate; remaining segments with one tergal and two sternal plates (**Figures 5A–D**, **6A–J**). Maximum sternal width at segment 6, almost constant throughout the trunk, slightly tapering at the last trunk segments (**Figures 5A,B**, **6A**). Sternal cuticular plates wide in ratio of maximum sternal width to trunk length (MSW-6:TL average ratio = 32.81%), giving the animal a plump appearance (**Figures 5A,B**, **6A**). Middorsal elevations on segments 1–10, with intracuticular, butterfly-like atria of paradorsal sensory spots; middorsal elevation of segment 10 smaller and thinner than previous ones (**Figures 5B**, **6B,D,F,I**). Segments 1–10 with rounded glandular cell outlets in subdorsal and ventromedial positions (**Figures 5A–D**, **6B–J**). Segments 2–10 with paired cuticular ridges in laterodorsal and ventrolateral positions, the latter with adjacent, minute glandular cell outlets (**Figures 5A–D**, **6B–J**). Cuticular hairs not observed. Muscular scars very conspicuous in laterodorsal and ventromedial positions (**Figures 5A–D**, **6B–J**). Pachycycli and

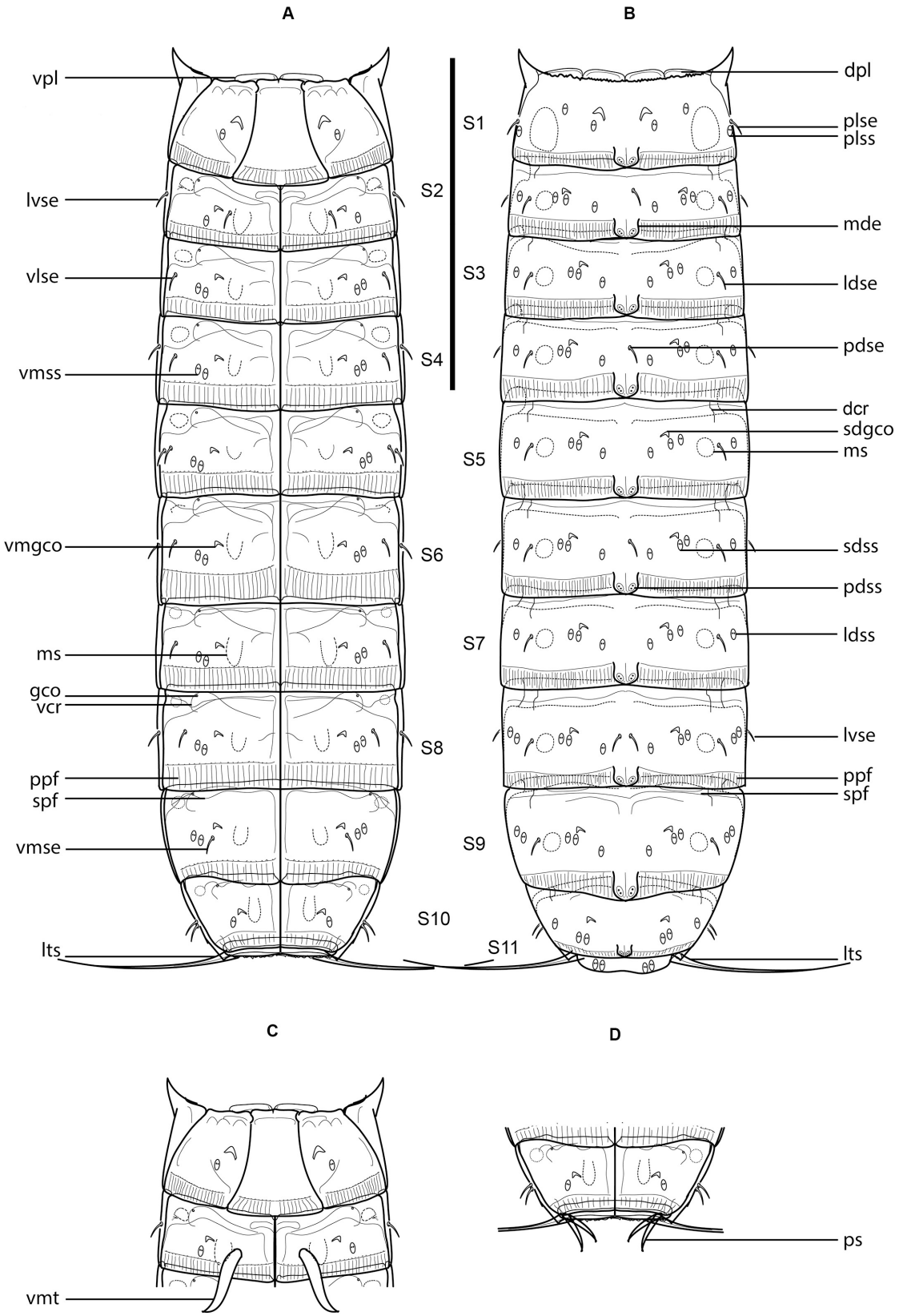

FIGURE 5 | Continued

FIGURE 5 | Line art illustrations of *Fujuriphyes hydra* sp. nov. **(A)** Female, ventral view; **(B)** female, dorsal view; **(C)** male, segments 1–2, ventral view; **(D)** male, segments 10–11, ventral view. Scale bar: 250 μm. Abbreviations: dcr, dorsal cuticular ridge; dpl, dorsal placid; gco, glandular cell outlet; ldse, laterodorsal seta; ldss, laterodorsal sensory spot; lts, lateral terminal spine; lvse, lateroventral seta; mde, middorsal elevation; ms, muscular scar; pdse, paradorsal seta; pdss, paradorsal sensory spot; plse, paralateral seta; plss, paralateral sensory spot; ppf, primary pectinate fringe; ps, penile spine; sdgco, subdorsal glandular cell outlet; sdss, subdorsal sensory spot; spf, secondary pectinate fringe; vcr, ventral cuticular ridge; vlse, ventrolateral seta; vmgco, ventromedial glandular cell outlet; vmse, ventromedial seta; vmss, ventromedial sensory spot; vpl, ventral placid; vmt, ventromedial tube.

ball-and-socket joints well-developed, thick, on segments 2–10 (**Figures 5A–D**, **6A**). Apodemes absent. Posterior margin of segments straight, showing primary pectinate fringes with weakly serrated free flaps (**Figures 5A–D**); secondary pectinate fringes not detectable under LM.

Segment 1 with middorsal elevation and associated butterfly-like intracuticular atria of the paradorsal sensory spots (**Figures 5B**, **6B**). Anterolateral margins of tergal plate as horn-like, distally pointed extensions (**Figures 5A–C**, **6A–C**). Anterior margin of tergal plate finely denticulate (**Figures 5B**, **6B**). Anterior margin of sternal plates with a wavy median ridge of cuticle (**Figures 5A,C**, **6A,C**). Midsternal plate trapezoidal, laterally extended at its base, with a lateral constriction near its anterior margin and a straight posterior margin (**Figures 5A,C**, **6A,C**). Paired setae in paralateral position (**Figures 5B**, **6B**). Sensory spots in paradorsal (one pair), subdorsal (two pairs), paralateral (one pair), and ventromedial (one pair) positions; all of them located at the anterior half of the cuticular plates except the paradorsal and paralateral ones (**Figures 5A–C**, **6B,C**).

Segment 2 with middorsal elevation as on the preceding segment (**Figures 5B**, **6D**). Unpaired seta in paradorsal position, and paired setae in laterodorsal and lateroventral positions; females with paired, sexually dimorphic setae in ventromedial position (**Figures 5A–C**, **6D,E**). Sensory spots in paradorsal (one pair), subdorsal (three pairs), laterodorsal (one pair), and ventromedial (one pair) positions (**Figure 5A–C**, **6D,E**). Males with sexually dimorphic tubes in ventromedial position (**Figure 5C**).

Segment 3 with middorsal elevation as on preceding segments (**Figures 5B**, **6D**). Paired setae in laterodorsal and ventrolateral positions (**Figures 5A,B**, **6D,E**). Sensory spots in paradorsal (one pair), subdorsal (three pairs), laterodorsal (one pair), and ventromedial (two pairs) positions (**Figures 5A,B**, **6D,E**). Subdorsal sensory spots more mesial than those of segment 2; ventromedial sensory spots closely located to each other (**Figures 5A,B**, **6D,E**).

Segment 4 with middorsal elevation as on preceding segments (**Figure 5B**). Unpaired seta in paradorsal position, and paired setae in laterodorsal, lateroventral, and ventrolateral positions, the former aligned with those of segment 3 (**Figures 5A,B**). Sensory spots in paradorsal (one pair), subdorsal (three pairs), laterodorsal (one pair), and ventromedial (two pairs) positions (**Figures 5A,B**).

Segment 5 similar to segment 3 in the arrangement of cuticular elevation, setae, and sensory spots, but with two pairs of ventrolateral setae, situated very close to each other (**Figures 5A,B**, **6F,G**).

Segment 6 similar to segment 4 in the arrangement of cuticular elevation, setae, and sensory spots (**Figures 5A,B**, **6F,G**).

Segment 7 similar to segment 3 in the arrangement of cuticular elevation, setae, and sensory spots (**Figures 5A,B**).

Segment 8 with middorsal elevation as on preceding segments (**Figures 5B**, **6I**). Paired setae in paradorsal, laterodorsal, lateroventral, and ventrolateral positions, the latter more mesial than those of previous segments but still in ventrolateral position (**Figures 5A,B**, **6I,J**). Sensory spots in paradorsal (one pair), subdorsal (three pairs), laterodorsal (two pairs), and ventromedial (two pairs) positions (**Figures 5A,B**, **6I,J**).

Segment 9 with middorsal elevation as on preceding segments (**Figures 5B**, **6I**). Paired setae in laterodorsal and ventromedial positions (**Figure 5A,B**, **6I,J**). Sensory spots in paradorsal (one pair), subdorsal (three pairs), laterodorsal (two pairs), and ventromedial (two pairs) positions (**Figure 5A,B**, **6I,J**). Nephridiopores not observed.

Segment 10 with middorsal elevation smaller and thinner than previous ones (**Figures 5B**, **6H**). Two pairs of setae in lateroventral position (**Figure 5B**). Sensory spots in paradorsal (one pair), subdorsal (two pairs), laterodorsal (one pair), and ventromedial (one pair) positions (**Figures 5A,B**, **6H**).

Segment 11 with two pairs of sensory spots in laterodorsal position (**Figure 5B**). Males with two pairs of sexually dimorphic penile spines and genital pores (**Figure 5D**). Lateral terminal spines long (LTS:TL average ratio = 30.97%), slender, narrow, apparently flexible (**Figures 5A,B**, **6A**).

Associated kinorhynch fauna

Fujuriphyes hydra sp. nov. co-occurred with the species *E. unispinosus* and *Ryuguderes* sp. in the analyzed samples.

Class Cyclorhagida (Zelinka, 1896) Sørensen et al., 2015.
Family Echinoderidae Zelinka, 1894.
Genus *Fissuroderes* Neuhaus and Blasche, 2006.

Fissuroderes cthulhu sp. nov.

urn:lsid:zoobank.org:act:8C27FAF4-0CD2-4767-9FE3-F46DEDDE9147 (**Figures 7–9**).

Material examined

Holotype, adult female, collected in October 2014 at Mahavavy area, Mozambique Channel, western Indian Ocean (−15° 32.532′, 45° 42.894′) at 775 m depth; mounted in Fluoromount G®, deposited at NHMD under accession number: 669727. Paratypes, five adult males and four adult females, with same collecting data as holotype; mounted in Fluoromount G®, deposited at NHMD under accession numbers: 669728–669736. Nineteen additional specimens mounted for LM, same collecting data as type material, deposited at NHMD under accession numbers: 669737–669755; one additional specimen mounted for

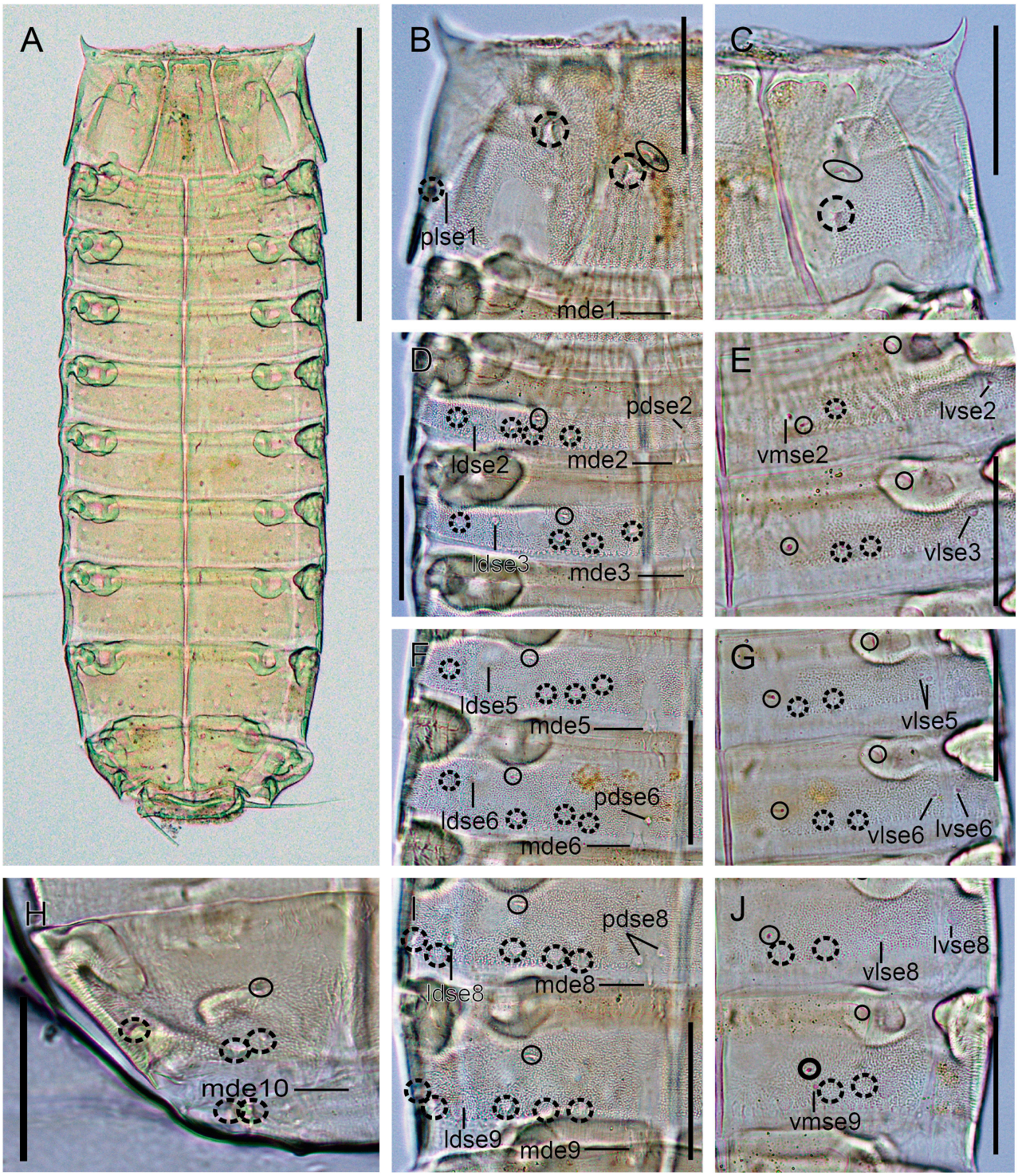

FIGURE 6 | Light micrographs showing trunk overview and details in the main trunk cuticular appendages of female holotype NHMD 669766 of *Fujuriphyes hydra* sp. nov. **(A)** Ventral overview of trunk; **(B)** middorsal to paralateral view on right half of tergal plate of segment 1; **(C)** ventrolateral to ventromedial view on left half of sternal plates of segment 1; **(D)** middorsal to laterodorsal view on right half of tergal plates of segments 2–3; **(E)** left sternal plates of segments 2–3; **(F)** middorsal to laterodorsal view on right half of tergal plates of segments 5–6; **(G)** left sternal plates of segments 5–6; **(H)** middorsal to laterodorsal view on right half of tergal plate of segment 10; **(I)** middorsal to laterodorsal view on right half of tergal plate of segments 8–9; **(J)** left sternal plates of segments 8–9. Scale bars: **(A):** 250 μm; **(B–J)**: 62 μm. Abbreviations: ldse, laterodorsal seta; mde, middorsal elevation; pdse, paradorsal seta; plse, paralateral seta; vlse, ventrolateral seta; vmse, ventromedial seta; numbers after abbreviations indicate corresponding segment; sensory spots are marked as dashed circles (except paradorsal ones), and glandular cell outlets as closed circles.

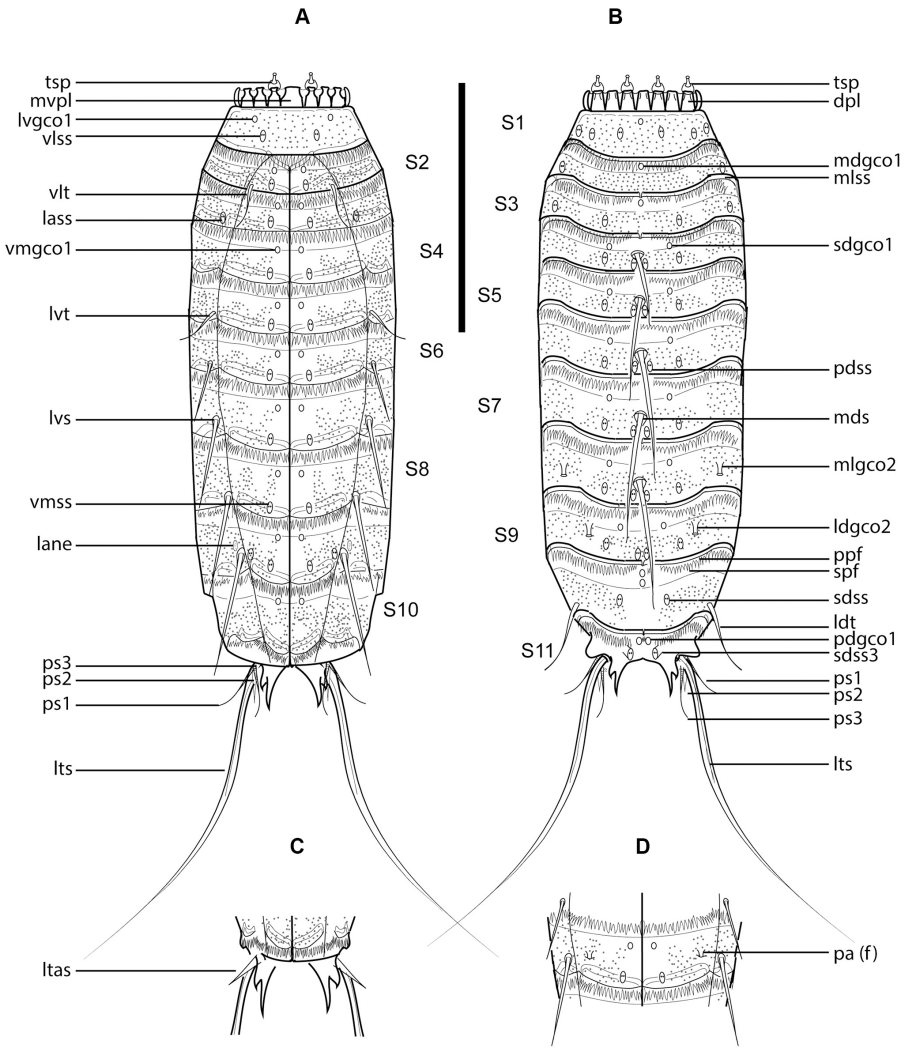

FIGURE 7 | Line art illustrations of *Fissuroderes cthulhu* sp. nov. **(A)** Male, ventral view; **(B)** male, dorsal view; **(C)** female, segments 10–11, ventral view; **(D)** female, segment 7, ventral view. Scale bar: 250 μm. Abbreviations: dpl, dorsal placid; f, female condition of sexually dimorphic character; lane, lateral accessory nephridiopore; lass, lateral accessory sensory spot; ldgco2, laterodorsal type 2 glandular cell outlet; ldss, laterodorsal sensory spot; ldt, laterodorsal tube; ltas, lateral terminal accessory spine; lts, lateral terminal spine; lvgco1, lateroventral type 1 glandular cell outlet; lvs, lateroventral spine; lvt, lateroventral tube; mdgco1, middorsal type 1 glandular cell outlet; mds, middorsal spine; mlgco2, midlateral type 2 glandular cell outlet; mlss, midlateral sensory spot; mvpl, midventral placid; pa, papilla; pdgco1, paradorsal type 1 glandular cell outlet; pdss, paradorsal sensory spot; ppf, primary pectinate fringe; ps, penile spine (followed by number of corresponding pair); sdgco1, subdorsal type 1 glandular cell outlet; sdss, subdorsal sensory spot; sdss3, subdorsal type 3 sensory spot; spf, secondary pectinate fringe; tsp, trichoscalid plate; vlss, ventrolateral sensory spot; vlt, ventrolateral tube; vmgco1, ventromedial type 1 glandular cell outlet; vmss, ventromedial sensory spot.

SEM, same collecting data as type material, deposited at the Meiofauna Collection of the UCM.

Diagnosis

Fissuroderes with spines in middorsal position on segments 4–8 and in lateroventral position on segments 6–9, increasing progressively in length toward the posterior segments; broad, elongated, and distally pointed tubes in ventrolateral position on segment 2, in lateroventral position on segment 5, and in laterodorsal position on segment 10. Tergal extensions of segment 11 elongated, distally bifurcated, with pointed tips. Type 2 glandular cell outlets in midlateral position on segment 8 and in laterodorsal position of segment 9. Females with sexually dimorphic papillae in ventrolateral position on segment 7.

Etymology

The species is named after the fictional cosmic entity Cthulhu, created by the American writer of horror fiction H.P. Lovecraft (1890-1937) and firstly introduced in the short story "The Call of Cthulhu," published in 1928. Considered a Great Old One within the pantheon of Lovecraftian cosmic entities, Cthulhu is a gigantic being of great power described as looking like an octopus or a dragon that lies in a death-like torpor in the sunken city of R'lyeh.

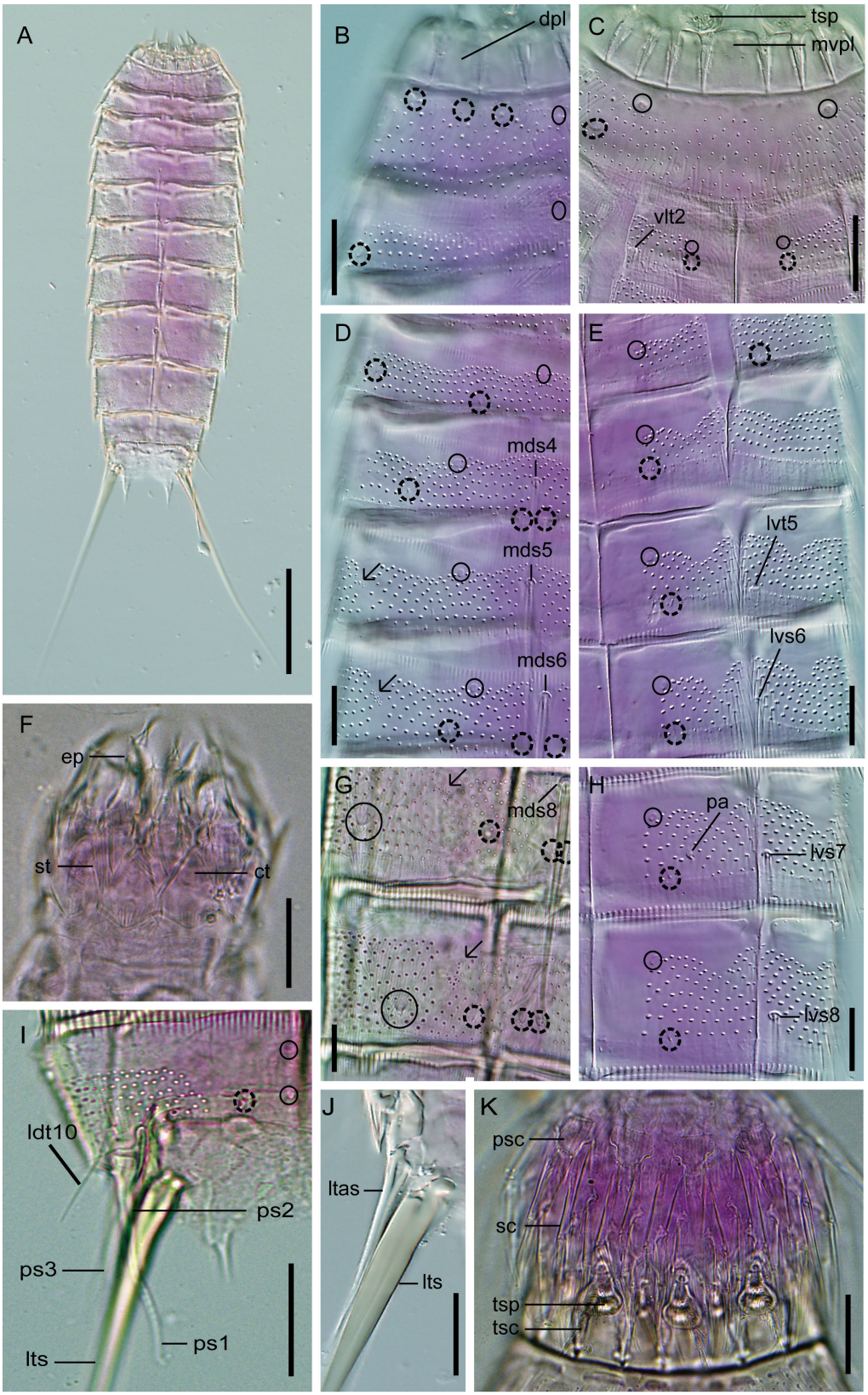

FIGURE 8 | Continued

FIGURE 8 | Light micrographs showing trunk overview and details in the head, neck, and main trunk cuticular characters of female holotype NHMD 669727 **(A–E,H,J)** and male paratype NHMD 669728 **(F,G,I,K)** of *Fissuroderes cthulhu* sp. nov. **(A)** Dorsal overview of trunk; **(B)** neck and middorsal to midlateral view on right half of tergal plates of segments 1–2; **(C)** neck and sublateral to ventromedial view tergal and sternal plates of segments 1–2; **(D)** middorsal to midlateral view on right half of tergal plates of segments 3–6; **(E)** sublateral to ventromedial view on left half of tergal and sternal plates of segments 3–6; **(F)** mouth cone; **(G)** middorsal to midlateral view on right half of tergal plates of segments 8–9; **(H)** sublateral to ventromedial view on left half of tergal and sternal plates of segments 7–8; **(I)** middorsal to midlateral view on right half of tergal plate of segment 10; **(J)** lateral terminal accessory spine; **(K)** introvert. Scale bars: **(A):** 100 μm; **(B–K)**: 20 μm. Abbreviations: ct, cuticular thickening; dpl, dorsal placid; ep, end-piece of outer oral style; ldt, laterodorsal tube; ltas, lateral terminal accessory spine; lts, lateral terminal spine; lvs, lateroventral spine; lvt, lateroventral tube; mds, middorsal spine; mvpl, midventral placid; pa, female papilla; ps, penile spine (followed by number of corresponding pair); psc, primary spinoscalid; sc, regular-sized scalid; st, spinous tuft of outer oral style; tsc, trichoscalid; tsp, trichoscalid plate; vlt, ventrolateral tube; numbers after abbreviations indicate corresponding segment; sensory spots are marked as dashed circles, and glandular cell outlets as closed circles; arrows indicate the muscular scars with several perforations as microsculpture.

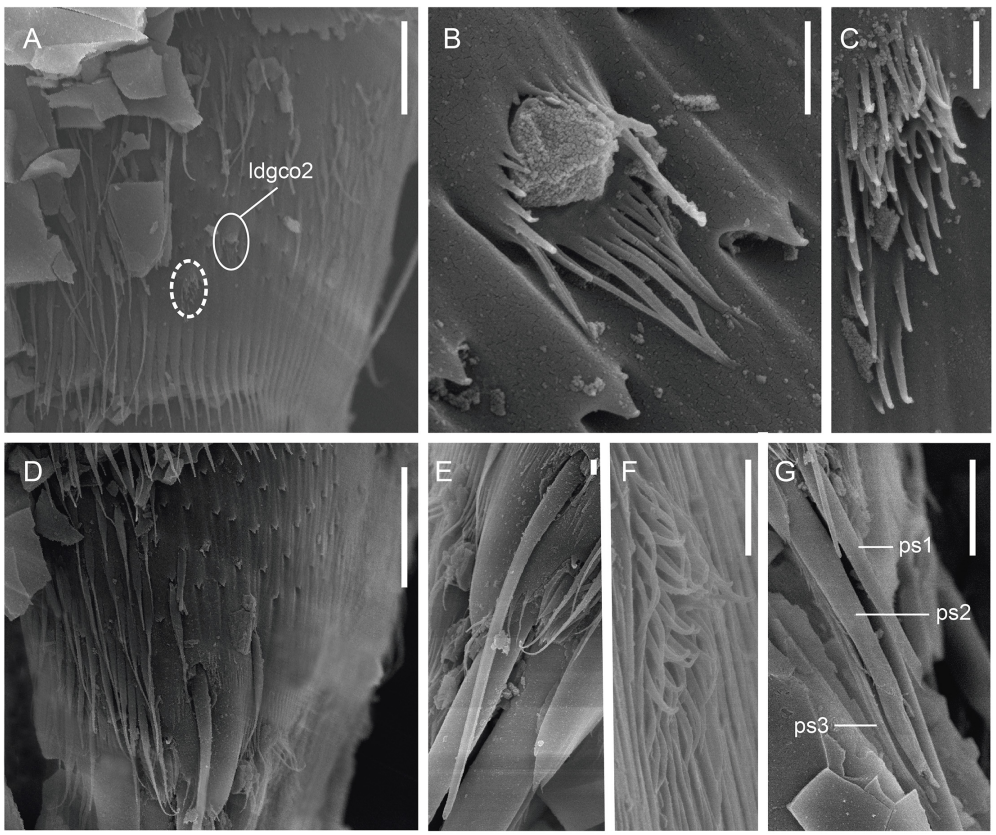

FIGURE 9 | Scanning electron micrographs showing some cuticular characters of segments 9–11 of a male of *Fissuroderes cthulhu* sp. nov. **(A)** Lateral view of segment 9; **(B)** detail of the laterodorsal type 2 glandular cell outlet of segment 9; **(C)** detail of the midlateral sensory spot of segment 9; **(D)** lateral view of segment 10; **(E)** detail of the laterodorsal tube of segment 10; **(F)** detail of the subdorsal sensory spot of segment 10; **(G)** detail of the penile spines of segment 11. Scale bars: **(A,D):** 10 μm; **(B,C,E–G)**: 1 μm. Abbreviations: ldgco2, laterodorsal type 2 glandular cell outlet; ps, penile spine (followed by number of corresponding pair); sensory spots are marked as dashed circles.

Description

See **Supplementary Table 1.5** for measurements and dimensions and **Supplementary Table 1.6** for summary of spine, tube, nephridiopore, glandular cell outlet, and sensory spot locations.

Head with retractable mouth cone and introvert (**Figures 8F,K**). Although some of the specimens have the introvert partially everted, oral styles and scalids tended to be collapsed when mounted for LM; furthermore, specimens for SEM were not suitable for head examination, so only some details on the exact number, arrangement, and morphology of oral styles and scalids can be provided.

Ring 00 of mouth cone with nine outer oral styles alternating in size between slightly larger and smaller ones (**Figure 8F**). Outer oral styles composed of two jointed subunits: a rectangular basal piece with a proximal sheath bearing a long, spinous tuft; and a triangular, curved end piece distally sharped (**Figure 8F**). Triangular, cuticular thickenings flanking the outer oral styles' bases (**Figure 8F**). Outer oral styles located anterior to each introvert sector, except in the middorsal section 6 where a style is missing.

Introvert with six transverse rings of scalids and 10 longitudinal sectors defined by the arrangement of the primary

spinoscalids. Ring 01 with 10 primary spinoscalids, larger than the remaining ones, laterally compressed, composed of a trapezoidal, wide basal sheath and a distal, elongated, flexible, distally blunt end piece (**Figure 8K**). The basal sheath bears two long, thread-like projections laterally and a median fringe of several long and flexible tips (**Figure 8K**). Rings 02–06 with regular-sized, laterally compressed scalids, much smaller than the primary spinoscalids, each one composed of a rectangular basal sheath carrying a median fringe and a distal, pointed end piece (**Figure 8K**). Exact arrangement of these scalids cannot be provided.

Neck with 16 trapezoidal placids, wider at bases, with a distinct joint between the neck and segment 1 (**Figures 7A,B**, **8B,C,K**). Midventral placid widest (ca. 17–19 μm wide at base), remaining ones narrower (ca. 12–13 μm wide at base) (**Figures 7A,B**, **8B,C,K**). Placids closely situated at base, distally separated by cuticular folds (**Figures 7A,B**, **8B,C,K**). A ring of six long, hairy trichoscalids associated with the placids of the neck is present, attached to large, bottle-like trichoscalid plates (**Figures 7A,B**, **8C,K**).

Trunk with 11 segments, triangular in cross-section (**Figures 7A,B**, **8A**). Segment 1 as closed cuticular ring, remaining ones with one tergal and two sternal cuticular plates (**Figures 7A–D**, **8A**). Tergal plates middorsally bulging. Maximum width at segment 6, progressively tapering toward the last trunk segments (**Figures 7A,B**, **8A**). Sternal plates relatively narrow compared to the total trunk length (MSW-6:TL average ratio = 22.3%), giving the animal a rectangular general appearance (**Figures 7A,B**, **8A**). Cuticular hairs present on segments 1–10, acicular, elongated, distally pointed, with rounded to oval-shaped perforation sites (**Figures 7A–D**, **8B–E,G,H**, **9A,D**). Cuticular hairs distributed in 5–7 wavy, transverse rows at the middle part of the plates on segments 2–9; in 6–7 straight, transverse rows almost covering the whole cuticular surface on segment 1; and segment 10 with 5–7 wavy, transverse rows at the middle part of the plates, from subdorsal to ventromedial regions (**Figures 7A–D**, **8B–E,G–I**). Muscular scars with several perforations as microsculpture throughout the trunk (**Figure 8D,G**). Posterior margin of segments 1–10 straight, showing a long, conspicuous primary pectinate fringe with a strong serration with bifid tips (**Figures 7A,B,D**, **8B–E,G,H**, **9A,D**). Secondary pectinate fringes on segments 2–11, with a very weak serration and usually hidden by the primary pectinate fringe of the previous segment (**Figures 7A,B,D**).

Segment 1 without spines and tubes. Unpaired type 1 glandular cell outlet in middorsal position, and paired type 1 glandular cell outlets in lateroventral position (**Figures 7A,B**, **8B,C**). Type 1 glandular cell outlets on this and remaining segments situated at the anterior half of the segment, sometimes hidden under the pectinate fringe of the previous segment. Paired sensory spots in subdorsal, laterodorsal, midlateral, and ventrolateral positions (**Figures 7A,B**, **8B,C**). Sensory spots on this and remaining segments composed of several long micropapillae and sometimes with a single, central cilium (**Figures 9C,F**).

Segment 2 with a pair of wide, flexible tubes in ventrolateral position (**Figures 7A**, **8C**). Tubes on this and remaining segments are composed of a short, rectangular, wide basal-piece and a flexible, elongated, distally pointed end piece that resembles an acicular spine in LM (**Figure 9E**). Unpaired type 1 glandular cell outlet in middorsal position, and paired type 1 glandular cell outlets in ventromedial position (**Figures 7A,B**, **8B,C**). Paired sensory spots in midlateral and ventromedial positions (**Figures 7A,B**, **8B,C**).

Segment 3 without spines and tubes. Unpaired type 1 glandular cell outlet in middorsal position, and paired type 1 glandular cell outlets in ventromedial position (**Figures 7A,B**, **8D,E**). Paired sensory spots in subdorsal, midlateral, lateral accessory, and ventromedial positions (**Figures 7A,B**, **8D,E**).

Segment 4 with a middorsal spine not exceeding the posterior edge of the following segment (**Figures 7B**, **8D**). Spines on this and remaining segments are acicular and flexible, increasing in length toward the end of the trunk throughout both the middorsal and lateroventral series (**Figures 7A,B**, **8D,E,G,H**). Paired type 1 glandular cell outlets in subdorsal and ventromedial positions (**Figures 7A,B**, **8D,E**). Paired sensory spots in paradorsal, laterodorsal, and ventromedial positions (**Figures 7A,B**, **8D,E**).

Segment 5 with a middorsal spine reaching the posterior edge of the following segment, and paired lateroventral tubes (**Figures 7A,B**, **8D,E**). Paired type 1 glandular cell outlets in subdorsal and ventromedial positions (**Figures 7A,B**, **8D,E**). Paired sensory spots in paradorsal, subdorsal, and ventromedial positions (**Figures 7A,B**, **8D,E**).

Segment 6 with a middorsal spine exceeding the posterior edge of the following segment, and paired lateroventral spines (**Figures 7A,B**, **8D,E**). Paired type 1 glandular cell outlets in subdorsal and ventromedial positions (**Figures 7A,B**, **8D,E**). Paired sensory spots in paradorsal, subdorsal, and ventromedial positions (**Figures 7A,B**, **8D,E**).

Segment 7 similar to segment 6 in the arrangement of spines, type 1 glandular cell outlets, sensory spots, and cuticular hairs, as well as in the morphology of the posterior margin of segment, primary and secondary pectinate fringes, except females that have sexually dimorphic papillae in ventrolateral position (**Figures 7A,B,D**, **8H**).

Segment 8 with a middorsal spine exceeding the posterior edge of the following segment, and paired lateroventral spines (**Figures 7A,B**, **8G,H**). Paired type 1 glandular cell outlets in subdorsal and ventromedial positions, and paired type 2 glandular cell outlets in midlateral position (**Figures 7A,B**, **8G,H**). Type 2 glandular cell outlets consist of a big, elevated pore surrounded by a single ring of long micropapillae (**Figure 9B**). Paired sensory spots in paradorsal, subdorsal, and ventromedial positions (**Figures 7A,B**, **8G,H**).

Segment 9 with paired lateroventral spines (**Figure 7A**). Paired type 1 glandular cell outlets in subdorsal and ventromedial positions, and paired type 2 glandular cell outlets in laterodorsal position (**Figures 7A,B**, **8G**, **9B**). Paired sensory spots in paradorsal, subdorsal, and ventromedial positions (**Figures 7A,B**, **8G**, **9C**). Nephridiopores as small sieve plates in lateral accessory position (**Figure 7A**).

Segment 10 with paired laterodorsal tubes (**Figures 7B**, **8I**, **9E**). Two unpaired type 1 glandular cell outlets in middorsal

position, and paired type 1 glandular cell outlets in ventromedial position (**Figures 7A,B**, **8I**). Paired sensory spots in subdorsal position (**Figures 7B**, **8I**, **9F**).

Segment 11 with type 1 glandular cell outlets in paradorsal position and type 3 sensory spots in subdorsal position (**Figure 7B**). Slender, flexible lateral terminal spines (**Figures 7A,B**, **8A,I,J**). Females with paired short, robust lateral accessory spines (LTAS:LTS average ratio = 28.4%) (**Figures 7C**, **8J**). Males with three pairs of penile spines: first and third pairs long, flexible and crenulated, second pair shorter, robust and superficially smooth (**Figures 7A,B**, **8I**, **9G**). Tergal extensions of segment 11 elongated, distally bifurcated, with pointed tips (**Figures 7A–C**, **8I**). Sternal plates distally rounded (**Figures 7A,C**).

Associated kinorhynch fauna

Fissuroderes cthulhu sp. nov. co-occurred with *Condyloderes* sp., *E. unispinosus* and *F. dagon* sp. nov. in the analyzed samples.

Community Structure Along the Vertical Profile and Intra-Habitats Comparison

Densities outside the pockmarks are low and significantly decrease from the upper to the bottom sediment layers (p = 0.0242), varying more gradually than those inside the pockmarks. Densities significantly vary along the vertical profile inside the pockmarks (p = 0.0117), reaching a peak in layer 1–2 cm (means of ca. 34 specimens per 10 cm^2 at MTB06 and 4 specimens per 10 cm^2 at MTB1), and strongly decreasing from this depth (**Table 1** and **Figures 10**, **11**). Likewise, species richness outside the pockmarks is low and changes significantly with sediment depth (p = 0.0389), having its highest value in the uppermost layer, 0–1 cm (means of ca. 1 species at both MTB2 and MTB03), and no specimens in the deepest layers, 3–4 and 4–5 cm (**Table 1** and **Figure 10**). Species richness is more stable along the vertical profile inside the pockmarks, and no significant differences are observed. The highest values are found in the second sediment layer (means of ca. 3 species at MTB06 and ca. 1 species in MTB1), and kinorhynchs are still present in the bottom layers (highest means at MTB06 of ca. 2 and 1 species at 3–4 and 4–5 cm depth, respectively) (**Table 1** and **Figure 10**).

Considering the whole cores, analyses between sites of the same habitat found no differences comparing sites outside the pockmarks (density, p = 0.5066; richness, p = 0.5002), or between the pockmark sites (density, p = 0.1266; richness, p = 0.0722), except for the species assemblage between the two pockmark sites (see below).

Inter-Habitats Comparison

Both habitats are similar in terms of species richness (p = 0.6831), with means of ca. 1–2 species outside the pockmarks (per site: ca. 2 species at MTB03 and 1 species at MTB2), and means of ca. 2 species inside the pockmarks (per site: ca. 3 species at MTB06 and 1 species at MTB1) (**Table 2** and **Figure 12**). However, kinorhynchs show a significant higher density inside the pockmarks (p = 0.0039), with means of ca. 35–36 specimens per 10 cm^2 inside the pockmarks (per site: 56 specimens at

TABLE 1 | Species richness and specimen abundance of Kinorhyncha present at the study sites.

		OUTSIDE POCKMARK MTB03					OUTSIDE POCKMARK MTB2					INSIDE POCKMARK MTB06					INSIDE POCKMARK MTB1				
	Sediment layer	A	B	C	X	Total	A	B	C	X	Total	A	B	C	X	Total	A	B	C	X	Total
Species Richness	0–1	1	0	2	1 ± 1	3	0	3	1	1.3 ± 1.5	3	-	2	2	2 ± 0	4	0	1	1	0.7 ± 0.6	2
	1–2	4	0	1	1.7 ± 2.1	5	0	0	0	0	0	1	3	4	2.7 ± 1.5	8	2	1	1	1.3 ± 0.6	4
	2–3	1	0	0	0.3 ± 0.6	1	0	0	0	0	0	2	1	2	1.7 ± 0.6	5	0	1	1	0.7 ± 0.6	2
	3–4	0	0	0	0	0	0	0	0	0	0	2	2	2	2 ± 0	6	0	0	1	0.3 ± 0.6	1
	4–5	0	0	0	0	0	0	0	0	0	0	2	1	1	1.3 ± 0.6	4	0	0	1	0.3 ± 0.6	1
Abundance	0–1	2	0	4	2 ± 2	6	0	3	1	1.3 ± 1.5	4	-	44	24	34 ± 14.1	68	0	46	15	20.3 ± 23.5	61
	1–2	11	0	3	4.7 ± 5.7	14	1	1	0	0.7 ± 0.6	2	84	16	210	103.3 ± 98.4	310	7	24	9	13.3 ± 9.3	40
	2–3	2	0	2	1.3 ± 1.2	4	0	0	0	0	0	19	8	68	31.7 ± 31.9	95	6	9	5	6.7 ± 2.1	20
	3–4	0	0	0	0	0	0	0	0	0	0	10	4	10	8 ± 3.5	24	12	1	1	4.7 ± 6.4	14
	4–5	0	0	0	0	0	0	0	0	0	0	2	1	4	2.3 ± 1.5	7	2	0	1	1 ± 1	3
Density (ind/10 cm^2)	0–1	0.7	0	1.3	0.7 ± 0.7		0	1	0.3	0.43 ± 0.51		-	14.6	8	11.3 ± 4.7		0	15.2	5	6.7 ± 7.7	
	1–2	3.6	0	1	1.5 ± 1.8		0.3	0.3	0	0.2 ± 0.17		27.8	5.3	69.6	34.2 ± 32.6		2.3	8	3	4.4 ± 3.1	
	2–3	0.7	0	0.7	0.5 ± 0.4		0	0	0	0		6.3	2.7	22.5	10.5 ± 10.5		2	3	1.7	2.2 ± 0.68	
	3–4	0	0	0	0		0	0	0	0		3.3	1.3	3.3	2.6 ± 1.1		4	0.3	0.3	1.5 ± 2.1	
	4–5	0	0	0	0		0	0	0	0		0.7	0.3	1.3	0.77 ± 0.5		0.7	0	0.3	0.33 ± 0.35	

Data are specified by cores and layers along the vertical profile. Total numbers show the data merging the information of the three cores. X refers to average values ± standard deviation.

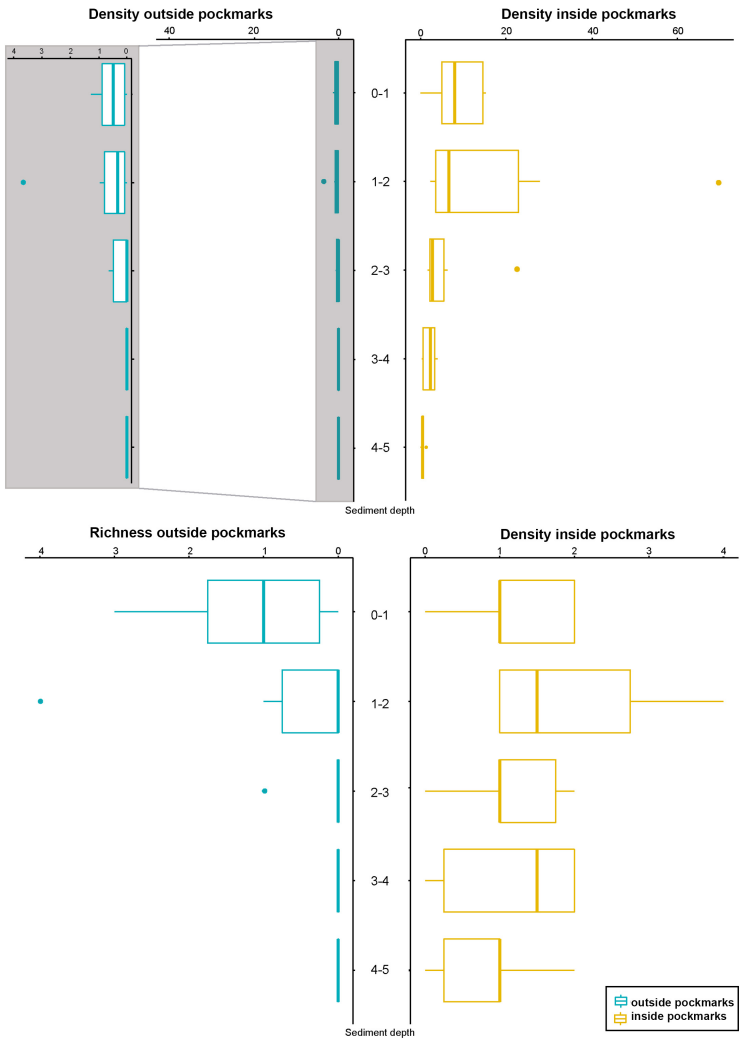

FIGURE 10 | Kinorhynch density and richness along the vertical profile of the two study habitats, inside pockmark (yellow) and outside pockmark (blue). Image enlargement of density outside the pockmark is provided to allow discerning variation of kinorhynch densities along the vertical profile. Boxplots represent the median value (horizontal line within the box), the distributions of 50% of the data (the box), and the highest and lowest values within 95% of the distribution (the whisker).

MTB06 and 15 specimens at MTB1) vs. means of ca. 1–2 specimens per 10 cm^2 outside the pockmarks (per site: ca. 3 specimens per 10 cm^2 at MTB03 and 0 specimens at MTB2) (**Table 2** and **Figures 11**, **12**). Juveniles were always present and relatively abundant both inside and outside the pockmarks, with means of ca. 3–4 specimens per 10 cm^2 outside (per site: ca. 5 specimens, 20.8% of the total kinorhynch abundance at MTB03 and 2 specimens, 33.3% at MTB2) and means of ca. 30–31 specimens per 10 cm^2 inside the pockmarks (per site: ca. 169 specimens, 33.5% of the total kinorhynch abundance at MTB06 and 92 specimens, 65.2% at MTB1) (**Table 2** and **Figure 12**).

It appears that most of the species are restricted to one of the studied habitats, except *Condyloderes* sp. and *E. unispinosus* Yamasaki et al., 2018b that are present both outside and inside the pockmarks. *E. unispinosus* is the dominant species inside the pockmarks (63.1% of the total adult kinorhynch community), followed far behind by *Fi. cthulhu* sp. nov. (15% of the adult community), *Echinoderes hviidarum* Sørensen et al., 2018 (11.8% of the adult community) and *F. dagon* sp. nov. (6.6% of the adult community) (**Table 2** and **Figure 12**). All the referred species were recovered only at the pockmark site MTB06, except for *E. hviidarum* that only appeared at MTB1 (**Table 2** and **Figure 12**). The remaining species were recovered only at one of the sites in low number: *Echinoderes apex* Yamasaki et al. (2018c), *Echinoderes* cf. *dubiosus*, *Echinoderes* sp., *Ryuguderes* sp., and *F. hydra* sp. nov. outside the pockmarks; and *Sphenoderes* cf. *indicus* as a singleton inside the pockmark MTB1 (**Table 2** and **Figure 12**).

Differences in community composition between the two study habitats, inside and outside the pockmarks, were observed (occurrence: $p = 0.005$, $F.Model = 3.8761$, $R^2 = 0.222$; abundance: $p = 0.003$, $F.Model = 3.8926$, $R^2 = 0.235$). Moreover, H_2S

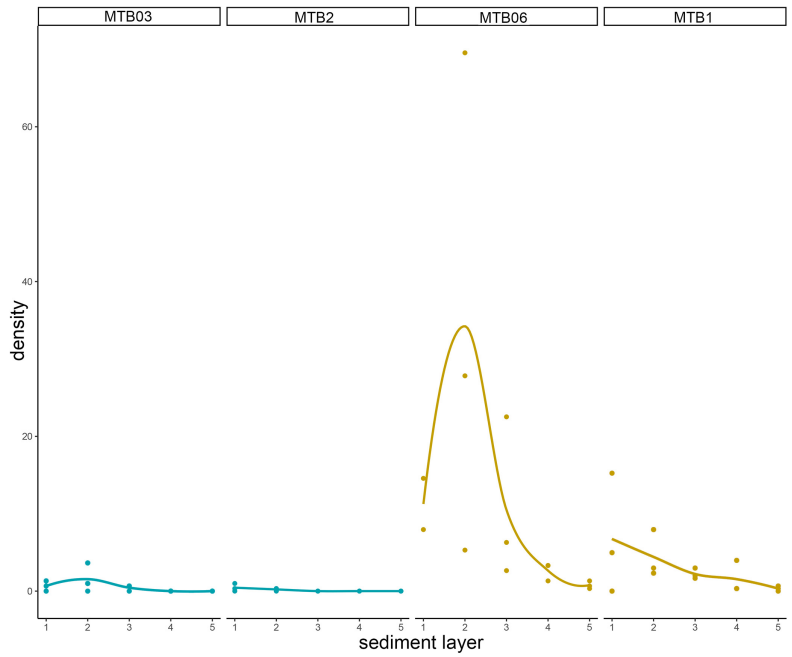

FIGURE 11 | Kinorhynch total density (including both adults and juveniles) along the vertical profile of the four study sites: MTB03 and MTB2 as outside pockmark sites (blue), and MTB06 and MTB1 (purple) as inside pockmark sites (yellow). Layers per core were determined as follows: layer 1 (0–1 cm), layer 2 (1–2 cm), layer 3 (2–3 cm), layer 4 (3–4 cm), and layer 5 (4–5 cm).

was found as a covariate explanatory variable (occurrence: $p = 0.001$, *F.Model* = 6.6067, $R^2 = 0.3779$; abundance: $p = 0.001$, *F.Model* = 5.6791, $R^2 = 0.343$). Differences in community composition were found between the two study pockmarks as well (occurrence: $p = 0.001$, *F.Model* = 44.255, $R^2 = 0.678$; abundance: $p = 0.001$, *F.Model* = 18.3670, $R^2 = 0.467$). None of the analyses showed significant differences to discriminate between sites outside the pockmarks. PCA for illustrating kinorhynch trends in community composition discriminated among sites: PC2 distinguished between sites located inside and outside the pockmarks, whereas PC1 discriminated between the two pockmarks (**Figure 13**). PC1 explained 39.8% of the variance and was mainly affected by the high abundance of *E. hviidarum* at the pockmark site MTB1 (site with the highest concentrations of H_2S and detection of CH_4), whereas *E. unispinosus* followed by *Fi. cthulhu* sp. nov. distinguished the pockmark site MTB06 (site with emission of CH_4 only, H_2S not detected), and PC2 explained 25.7% of the variance, with *Condyloderes* sp., *Echinoderes* cf. *dubious*, and *Ryuguderes* sp. characterizing the sites located outside the pockmarks and *E. unispinosus* and *E. hviidarum* characterizing the sites inside the pockmarks (**Figure 13**). We are aware that a larger total variance explained by the two PCAs would have been desirable and therefore other factors not included in the present study could be responsible for the remaining percentage of variance, but still the studied pockmark conditions explained some differences in the kinorhynch community composition between both pockmarks and between pockmarks and sites outside pockmarks.

DISCUSSION

Remarks on Diagnostic and Taxonomic Features of *F. dagon* sp. nov. and *F. hydra* sp. nov.

The two new species of *Fujuriphyes* agree with the main diagnostic characters of the genus, including the presence of ventrolateral setae on segment 5 and on additional segments from segment 3 to 9 where ventromedial setae are absent, as well as long lateral terminal spines (LTS:TL average ratio > 30%) (Sánchez et al., 2016). Until now, the genus was composed of seven species: three from the Caribbean Sea, *Fujuriphyes dalii* Cepeda et al., 2019b, *F. deirophorus* (Higgins, 1983), and *F. distentus* (Higgins, 1983); one from the Gulf of Mexico, *F. viserioni* Sánchez et al., 2019a,b; one from the East China Sea, *F. longispinosus* Sánchez and Yamasaki, 2016; and two from the Mediterranean Sea, *F. ponticus* (Reinhard, 1881) and *F. rugosus* (Zelinka, 1928).

The presence of lateral terminal spines in both *F. dagon* sp. nov. and *F. hydra* sp. nov. easily allows their differentiation from *F. deirophorus* and *F. distentus* that lack these structures (Higgins, 1983).

The absence of middorsal cuticular specializations (processes or elevations) throughout the trunk in *F. dagon* sp. nov. is only shared with *F. dalii* (Cepeda et al., 2019b). However, both species may be easily distinguished by the arrangement of setae. *F. dalii* has a pair of paralateral setae on segment 1 (Cepeda et al., 2019b), which are absent in *F. dagon* sp. nov. The lateroventral

TABLE 2 | Kinorhyncha species identified at study sites.

	OUTSIDE POCKMARK MTB03					OUTSIDE POCKMARK MTB2					INSIDE POCKMARK MTB06					INSIDE POCKMARK MTB1				
Species	**A**	**B**	**C**	**X**	**Total**	**A**	**B**	**C**	**X**	**Total**	**A**	**B**	**C**	**X**	**Total**	**A**	**B**	**C**	**X**	**Total**
Condyloderes sp.	0	0	0	0	0	0	1	1	0.67 ± 0.58	2	0	0	1	0.33 ± 0.58	1	0	0	0	0	0
Echinoderes apex	1	0	0	0.33 ± 0.58	1	0	0	0	0	0	0	0	0	0	0	0	0	0	0	0
Echinoderes cf. *dubiosus*	0	0	3	1 ± 1.7	3	0	1	0	0.33 ± 0.58	1	0	0	0	0	0	0	0	0	0	0
Echinoderes hviidarum	0	0	0	0	0	0	0	0	0	0	0	0	0	0	0	5	24	16	15 ± 9.5	45
Echinoderes unispinosus	2	0	1	1 ± 1	3	0	0	0	0	0	77	24	151	84 ± 63.8	252	0	0	0	0	0
Echinoderes sp.	0	0	2	0.67 ± 1.2	2	0	0	0	0	0	0	0	0	0	0	0	0	0	0	0
Fissuroderes cthulhu sp. nov.	0	0	0	0	0	0	0	0	0	0	12	3	42	19 ± 20.4	57	0	0	0	0	0
Ryuguderes sp.	4	0	0	1.3 ± 2.3	4	0	1	0	0.33 ± 0.58	1	0	0	0	0	0	0	0	0	0	0
Sphenoderes cf. *indicus*	0	0	0	0	0	0	0	0	0	0	0	0	0	0	0	1	0	0	0.33 ± 0.58	1
Fujuriphyes dagon sp. nov.	0	0	0	0	0	0	0	0	0	0	0	6	19	8.3 ± 9.7	25	0	0	0	0	0
Fujuriphyes hydra sp. nov.	6	0	0	2 ± 3.5	6	0	0	0	0	0	0	0	0	0	0	0	0	0	0	0
Adult abundance	13	0	6	6.3 ± 6.5	19	0	3	1	1.3 ± 1.5	4	89	33	213	111.7 ± 92.11	335	6	24	16	15.3 ± 9	46
Total abundance	15	0	9	8.0 ± 7.6	24	1	4	1	2 ± 1.7	6	115	73	316	168 ± 129.9	504	27	80	31	46 ± 29.5	138
Total density (ind/10 cm^2)	5	0	3	2.6 ± 2.5		0.5	0.2	0.5	0.37 ± 0.15		38.1	24.2	105	55.6 ± 43		8.9	26.5	10.3	15.2 ± 9.8	
Total species richness	4	0	3	2.3 ± 2.1	6	0	3	1	1.3 ± 1.5	3	2	3	4	3 ± 1	4	2	1	1	1.3 ± 0.6	2

Abundance of each species is specified by cores and merging the data of the three cores in the total. Data are specified by cores and merging the data of the three cores. Total abundance includes adults and juvenile stages. X refers to average values ± standard deviation.

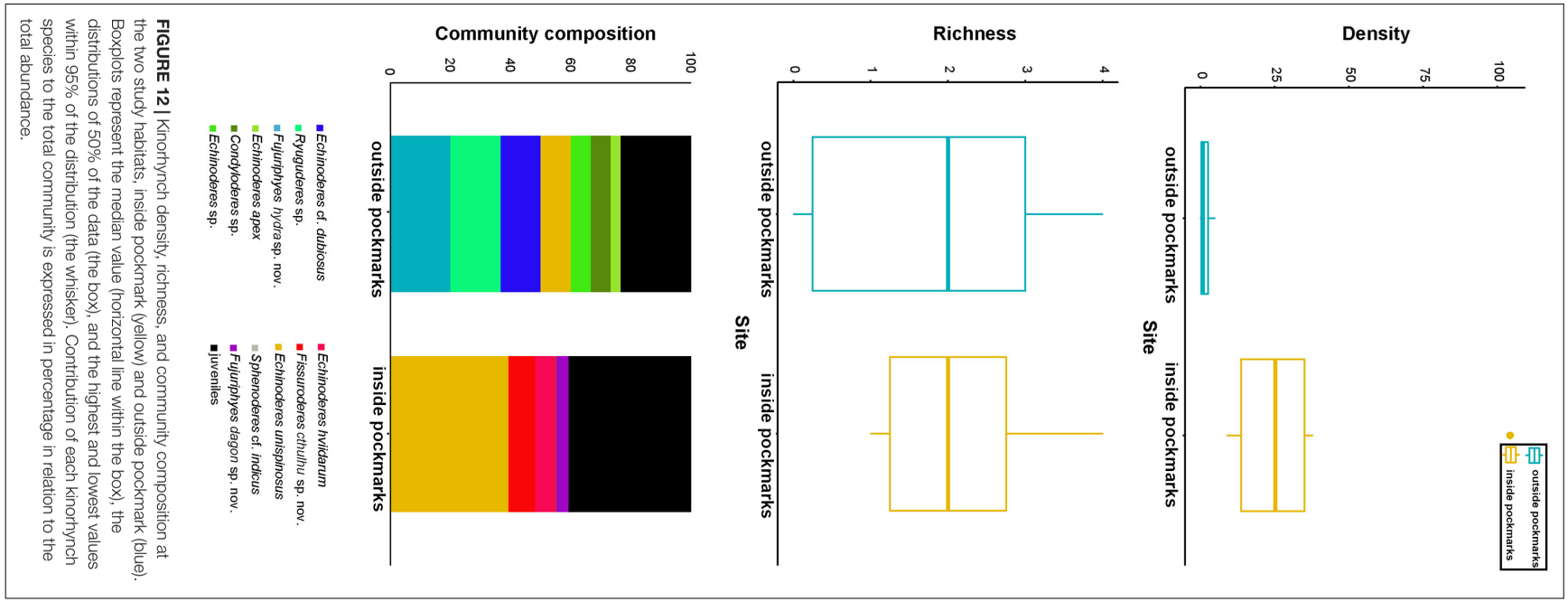

FIGURE 12 | Kinorhynch density, richness, and community composition at the two study habitats. inside pockmark (yellow) and outside pockmark (blue). Boxplots represent the median value (horizontal line within the box), the distributions of 50% of the data (the box), and the highest and lowest values within 95% of the distribution (the whisker). Contribution of each kinorhynch species to the total community is expressed in percentage in relation to the total abundance.

setae of *F. dalii* are only present on segments 2, 4, and 10 (Cepeda et al., 2019b), while those of *F. dagon* sp. nov. are present on all the even-numbered segments. *F. dagon* sp. nov. has ventrolateral setae on segment 2, which are absent in *F. dalii* sp. nov. (Cepeda et al., 2019b). Additionally, *F. dalii* possesses ventromedial setae on segments 8–9 (Cepeda et al., 2019b), whereas *F. dagon* sp. nov. lacks setae in ventromedial position throughout the trunk.

The presence of middorsal elevations throughout segments 1–10 in *F. hydra* is unique within the genus, as the remaining species possess a different arrangement of middorsal elevations. *F. ponticus* and *F. rugosus* bear these structures on segments 1–9; *F. viserioni*, on segment 3; and *F. longispinosus*, on segments 1–6 (Reinhard, 1881; Zelinka, 1928; Sánchez and Yamasaki, 2016; Sánchez et al., 2016, 2019b). Regarding the setae arrangement, *F. hydra* sp. nov. is most similar to *F. dalii* and *F. longispinosus*, as the three species possess two pairs of ventrolateral setae on segment 5 and a relatively low number of ventromedial setae. Thus, *F. dalii* has ventromedial setae on segments 8–9, and *F. longispinosus* bears these structures on segments 2 and 9 in both sexes (Sánchez et al., 2016; Cepeda et al., 2019b). *F. hydra* sp. nov. also has ventromedial setae on segments 2 and 9, but those of segment 2 are only present in females. Moreover, the two pairs of ventrolateral setae of segment 5 of *F. hydra* sp. nov. are situated very close together, a feature that has not been observed in the remaining congeners.

Remarks on Diagnostic and Taxonomic Features of *Fi. cthulhu* sp. nov.

Currently, the genus *Fissuroderes* is morphologically defined by the combination of one tergal and two sternal plates on segment 2 plus paired, sexually dimorphic ventral papillae in females (Herranz and Pardos, 2013), despite the fact that females of one of the species, *Fi. papai* Neuhaus and Blasche, 2006, lack these structures. The newly described species, *Fi. cthulhu* sp. nov., matches the aforementioned condition of sexually dimorphic papillae, as only females bear these structures in ventrolateral position on segment 7. *Polacanthoderes* is the only genus of the family Echinoderidae that shares the arrangement of cuticular plates of segment 2 with *Fissuroderes* (Claparède, 1863; Adrianov and Malakhov, 1999; Neuhaus and Blasche, 2006; Sørensen, 2008a; Herranz et al., 2012), but it is furthermore characterized by possessing unusual morphological features never found in the remaining kinorhynch genera, including acicular spines in subdorsal, laterodorsal, midlateral, ventrolateral, and ventromedial positions (Sørensen, 2008a). This led us to include the new species in the genus *Fissuroderes*. Nevertheless, a total-evidence systematic revision of the family Echinoderidae is needed in order to describe new reliable characters of the different genera (Sørensen, 2008b; Sørensen et al., 2015).

Regarding the spine and tube arrangements, *Fi. cthulhu* sp. nov. is most similar to *Fi. novaezealandia* Neuhaus and Blasche (2006) and *Fi. thermoi* Neuhaus and Blasche (2006), as the three species share the presence of middorsal spines on segments 4–8, lateroventral spines on segments 6–9, ventrolateral tubes on segment 2, and lateroventral tubes on segment 5 (Neuhaus and Blasche, 2006). However, *Fi. novaezealandia* lacks laterodorsal tubes on segment 10, which are present and easily recognizable in *Fi. thermoi* and *Fi. cthulhu* sp. nov. (Neuhaus and Blasche, 2006). The main morphological differences between *Fi. thermoi* and *Fi. cthulhu* sp. nov. are the arrangement of the type 2 glandular cell outlets and female papillae, and the shape of the tergal extensions. *Fissuroderes thermoi* possesses type 2 glandular cell outlets in midlateral position on segments 5, 6, 8, and 9 (females furthermore with papillae in ventromedial position of segment 7), and its tergal extensions are short and distally rounded (Neuhaus and Blasche, 2006), while *Fi. cthulhu* sp. nov. has type 2 glandular cell outlets in midlateral position on segment 8 and in laterodorsal position on segment 9 (females furthermore with papillae in ventrolateral position of segment 7), and its tergal extensions are long, bifurcated, and distally pointed.

New Kinorhynch Records

The species *E. apex*, *E.* cf. *dubiosus*, *E. hviidarum*, *E. unispinosus*, *Ryuguderes* sp., and *Sphenoderes* cf. *indicus* were also reported in the analyzed pockmark field for the first time. In addition, *Condyloderes* sp. and *Echinoderes* sp. were also recorded, but the material was badly preserved and did not allow us to identify them to the species level.

A single specimen of *E. apex* was found at MOZ01-MTB03 (outside pockmarks). The species is characterized by having spines in middorsal position on segments 4, 6, and 8 and in lateroventral position throughout segments 6–9, together with tubes in ventrolateral position on segment 2, lateroventral position on segment 5, and laterodorsal position on segment 10, and type 2 glandular cell outlets in subdorsal position on segment 2, sublateral position on segment 6, and lateral accessory position on segment 8 (Yamasaki et al., 2018c). Moreover, *E. apex* has a relatively short trunk, ranging from 165 to 215 μm, and long lateral terminal spines, ranging from 60.0 to 80.2% of the total trunk length (Yamasaki et al., 2018c). The specimen found in the present study agrees with these diagnostic characters (see **Supplementary Figure 2.1**), except the length of the lateral terminal spines that are slightly shorter than those of the type material, ranging from 54.5 to 56.0% of the total trunk length, but we do not consider this difference important enough to assign the specimen to a different species. *E. apex* has been reported in the Great Meteor Seamount (eastern Atlantic Ocean) at depths of 287–856 m (Yamasaki et al., 2018c). This finding supposes an extension of the distributional range of the species to the Mozambique Channel (Indian Ocean).

Three specimens of *Echinoderes* cf. *dubiosus* were recorded at MOZ01-MTB03 and one was recorded at MOZ04-MTB2 (outside pockmarks). *Echinoderes dubiosus* is characterized by having spines in middorsal position throughout segments 4–8 and in lateroventral position on segments 6–9 (with those of segment 9 extending beyond segment 11), as well as tubes in lateroventral position on segment 5, sublateral position on

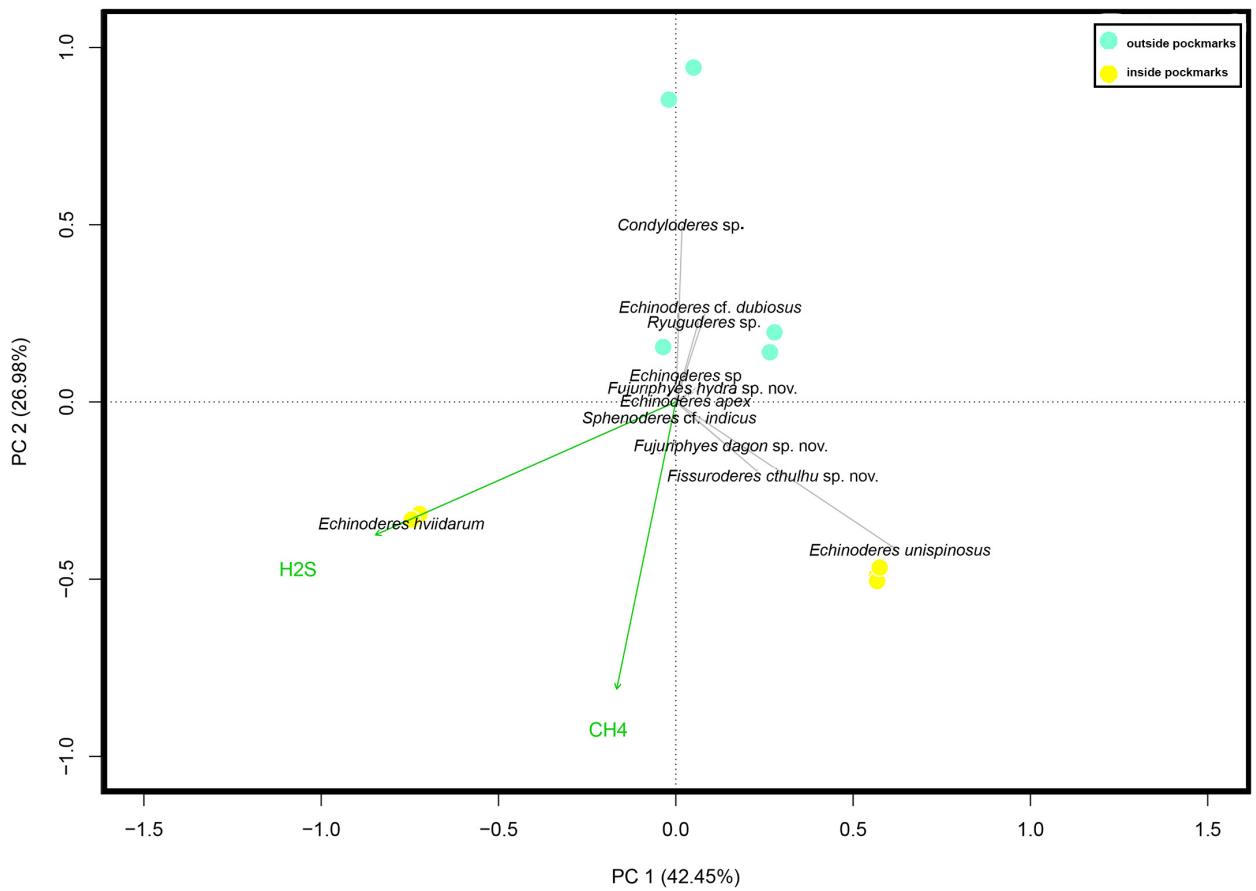

FIGURE 13 | Principal component analysis scaling two bi-plots based on Hellinger-transformed data on kinorhynch species composition considering the four study sites: two sites inside pockmarks (yellow) and two sites outside pockmarks (blue). Passive (*post hoc*) explanations of axis were conducted using environmental variables (CH_4, methane; and H_2S, hydrogen sulfide concentrations).

segment 8, and laterodorsal position on segment 10, and type 2 glandular cell outlets in midlateral position on segment 2 (Sørensen et al., 2018). The species also has middorsal cuticular structures on segment 9 forming a pore with a posterior papillary flap flanked by paired sensory spots (Sørensen et al., 2018). This last character was not observed in the specimens from the Mozambique Channel (see **Supplementary Figure 2.2**), which led us to tentatively identify them as *E.* cf. *dubiosus*. The species was previously known from the northern California (eastern Pacific Ocean) at 2702–3853 m depth (Sørensen et al., 2018), and this finding increases its bathymetrical and distributional range.

Echinoderes hviidarum was consistently found at MOZ04-MTB1 (within pockmark). The species has spines in middorsal position on segments 6 and 8 and lateroventral position throughout segments 6–9, as well as tubes in lateroventral position on segment 5, lateral accessory position on segment 8, and laterodorsal position on segments 9–10, and a middorsal protuberance on segment 11 (Sørensen et al., 2018). The specimens reported in the Mozambique Channel agree well with the aforementioned diagnostic characters of the species (see **Supplementary Figure 2.3**). *E. hviidarum* was exclusively reported off northern California (eastern Pacific Ocean) at 2702–3853 m depth (Sørensen et al., 2018), but with these findings, the bathymetrical and distributional range of the species is increased.

Echinoderes unispinosus was consistently reported at MOZ01-MTB03 (outside pockmarks) and MOZ01-MTB06 (within pockmark) and can be distinguished from its congeners by possessing spines in middorsal position on segment 4 and lateroventral position on segments 6–7, together with type 2 glandular cell outlets in midlateral position on segment 1; in subdorsal, laterodorsal, sublateral, and ventrolateral positions on segment 2; in lateral accessory position on segment 5; and in sublateral position on segment 8 (Yamasaki et al., 2018b). The species is furthermore characterized by having a narrow primary pectinate fringe with short tips throughout segments 1–10 and tergal extensions long, smoothly pointed (Yamasaki et al., 2018b). The specimens from the Mozambique Channel agree with these diagnostic characters of the species

(see **Supplementary Figure 2.4**), and the only morphological difference observed was the presence of subdorsal sensory spots on segment 4, which were not detected in the type material. *E. unispinosus* is known to possess a wide distributional range, being present in the northeast Atlantic Ocean, the northeast Pacific Ocean, and the Gulf of Mexico (Sørensen et al., 2018; Yamasaki et al., 2018b; Álvarez-Castillo et al., 2020). Now, its distributional range is furthermore increased to the Indian Ocean.

Three specimens from MOZ01-MTB03 and one from MOZ04-MTB02 (outside pockmarks) were tentatively assigned to *Ryuguderes* sp. This recently established genus of Campyloderidae can be distinguished from *Campyloderes* by having outer oral styles partially fused throughout the basal regions and free distal parts bearing lateral cuticular structures, as well as by the absence of lateroventral spines throughout the first trunk segments (Yamasaki, 2016). Currently, only a single species is known from the Ryukyu Islands (western Pacific Ocean), namely, *Ryuguderes iejimaensis* Yamasaki, 2016. The specimens from the Mozambique Channel seem to possess the diagnostic outer oral styles of *Ryuguderes*, but the lack of SEM material did not allow us to surely confirm this character. In addition, these specimens have important morphological discrepancies with *R. iejimaensis*, including the presence of a middorsal spine on segment 1, lateroventral spines on segment 3, a single pair of lateroventral spines on segment 5, females with middorsal spines on segment 10, and a different arrangement of sensory spots and glandular cell outlets (see **Supplementary Figure 2.5**).

A single specimen of *Sphenoderes* cf. *indicus* was found at MOZ04-MTB01 (within pockmark). *Sphenoderes indicus*, widely reported through the Bay of Bengal (Indian Ocean) at 6–40 m depth, is characterized by having acicular spines in middorsal position throughout segments 1–11 and lateroventral position on segments 3–9, as well as cuspidate spines in lateroventral position on segments 5 and 8–9, with those of segments 5 and 8 located more ventral than the acicular spines (Higgins, 1969). These characters were also found in the specimens from the Mozambique Channel (see **Supplementary Material 9**), but the arrangement of the sensory spots could not be completely determined because of the bad preservation of the specimens, which led us to tentatively identify them as *S.* cf. *indicus*. These findings increase the bathymetrical and distributional range of the species throughout the Indian Ocean.

Kinorhynch Community Structure and Composition

Our results show that kinorhynch density and community composition seem to be influenced by the environmental conditions of each study habitat, whereas similar values of richness were found in the inter-habitat comparison (**Figure 12**).

Kinorhynchs are more abundant inside the pockmarks, where environmental conditions are extreme due to reduced chemical compounds and the shortage of dissolved oxygen (Kumar, 2017; Pastor et al., 2020). Indeed, inside the pockmarks, hydrogen sulfide concentration increases with depth along the vertical profile while the dissolved oxygen plummets (Coull, 1988; Ritt et al., 2011; Ristova et al., 2015; Pastor et al., 2020). Specifically, most of the animals were found in the upper sediment layers (0–1 cm and 1–2 cm) (**Figure 10**). These layers are well-oxygenated (Coull, 1988; Pastor et al., 2020), and in one of the study pockmarks, there is a still relatively low concentration of hydrogen sulfide, a toxic reduced compound (Somero et al., 1989; Bagarinao, 1992; Giere, 2009). These findings agree with the hypothesis of Sánchez et al. (under review) and seem to evidence that the pockmark conditions enhance the abundance of Kinorhyncha, likely through the replacement with opportunistic, specialized species. These species would be able to cope with the pockmark conditions where other meiofaunal organisms cannot live (including other non-adapted species of Kinorhyncha), profiting about this and thriving rapidly (Ritt et al., 2010; Vanreusel et al., 2010; Sánchez et al., under review). This is also supported by the presence of a relatively high juvenile abundance inside the pockmarks, which shows that these species not only manage to survive under such extreme conditions but also are able to intensely flourish there. Indeed, certain groups of meiofauna, such as nematodes and harpacticoid copepods, can reach high peaks of abundance in extreme environments where competition with other taxa is lower, which makes their prosperity possible (Coull, 1985; Colangelo et al., 2001; Van Gaever et al., 2009; Zeppilli and Danovaro, 2009; Zeppilli et al., 2012, 2018). Alternatively, the elevated kinorhynch density, including the high number of juveniles, may be explained, in the context of pockmarks, as they are considered potential colonizers at sulfide seepages of deep sea vents (Mullineaux et al., 2012).

Additionally, pockmarks are rich in reduced compounds, resulting in higher chemosynthetic microbial densities that live in these habitats as hydrocarbon degraders, acting in the anaerobic oxidation of methane and sulfate reduction processes (Giovannelli et al., 2016). The bacterial mats form a major source of food for meiofauna, including kinorhynchs who likely feed on them (Neuhaus, 2013). Thus, pockmarks may also enhance high kinorhynch densities because of the abundant bacteria, also in those layers where the hydrogen sulfide concentration (formed as a waste product of the anaerobic respiration of reducing microorganisms) is still tolerable. However, as soon as the hydrogen sulfide concentration increases in the subsequent layers, it seems to turn toxic and both kinorhynch density and richness decrease (**Figure 10**).

Cold seeps also increase the spatial heterogeneity of the habitat through geochemical gradients, driving the distribution of the biological communities (Levin, 2005; Guillon et al., 2017). This fact furthermore supports the differences in the community composition between pockmarks and areas outside pockmarks' influence, so the greater availability of geochemically heterogeneous microhabitats inside the pockmark may enable the maintenance of a community made up of highly adapted kinorhynch species to the particular conditions of each pockmark.

Thus, even though a similar kinorhynch richness was found in areas under pockmark influence and outside pockmarks,

community composition drastically differs from one habitat to another (**Figures 12**, **13**), suggesting that only certain species are well-adapted and able to tolerate the extreme conditions of this kind of cold seeps, characterized by methane and hydrogen sulfide emissions, as was already confirmed for other meiofaunal groups (Vanreusel et al., 2010; Zeppilli et al., 2012, 2018). The pockmark conditions seem to prevent the survival of non-adapted species, with their consequent fading, as occur for *E. apex*, *E.* cf. *dubiosus*, *Echinoderes* sp., *F. hydra* sp. nov., and *Ryuguderes* sp., only found outside the pockmark sites.

Condyloderes sp., *E. hviidarum*, *E. unispinosus*, *Fi. cthulhu* sp. nov., *F. dagon* sp. nov., and *Sphenoderes* cf. *indicus* characterize the kinorhynch community in the areas under the pockmark's influence. Of these, only *Condyloderes* sp. and *E. unispinosus* seem to be generalistic species capable of living in both habitats, but their abundances are higher inside pockmarks by far. These two species, together with *E. hviidarum* and *Fi. cthulhu* sp. nov., do not simply survive under such harsh conditions but take advantage of a habitat with a likely lower competition for space and resources, flourishing there (Sánchez et al., under review). Additionally, the dissimilarity in kinorhynch community composition between the two study pockmarks is remarkable as well. *E. hviidarum* seems to be the most tolerant species to hydrogen sulfide as it largely dominated the community at the more active pockmark with higher concentrations of hydrogen sulfide. Indeed, *E. hviidarum* was also present in deep layers where the highest concentrations of hydrogen sulfide were detected. On the other hand, *E. unispinosus*, *Fi. cthulhu* sp. nov., and *F. dagon* sp. nov. only appeared in the pockmark with methane but without hydrogen sulfide emission (**Figure 13**). Therefore, methane and hydrogen sulfide, among other ecological factors, turn out to significantly drive kinorhynch community structure and composition, but we cannot conclude that all the aforementioned species are truthful bioindicators of cold seeps activity, as some of them were originally described from habitats free of seepages influence (Higgins, 1983; Sørensen et al., 2018; Yamasaki et al., 2018b). It remains to be clarified if the species described in the present article, *Fi. cthulhu* sp. nov. and *F. dagon* sp. nov., are only present in cold seepages or not.

CONCLUSION

Despite the fact that data interpretation of the present study must be taken with caution due to the reduced number of sampling sites and the possible effect of spatiotemporal variation among samples, we could make the following conclusions:

- Deep-sea environments host a highly biodiverse community of still undescribed species of Kinorhyncha.
- Kinorhynch richness is similar inside and outside the pockmarks, but the species composition completely changes because of exclusive species at both habitats.
- Contrarily to kinorhynch species richness, abundance is affected by the pockmarks' conditions, being higher within pockmarks than outside them. The extreme conditions of these habitats boost the kinorhynch abundance likely through the replacement with opportunistic specialized species, such as *E. hviidarum*, *E. unispinosus*, and *Fi. cthulhu* sp. nov., able to thrive rapidly under such features where competition is lower by far as hydrogen sulfide is toxic for most metazoans.

DATA AVAILABILITY STATEMENT

All datasets generated for this study are included in the article/**Supplementary Material**.

AUTHOR CONTRIBUTIONS

NS and DZ conceived the general idea of the study. DC, NS, and FP conducted the experimental process, and NS statistically analyzed the results. DC wrote the background and taxonomic part of the manuscript, and NS wrote the methods and the ecological part of the study. All the authors reviewed the manuscript.

FUNDING

This study was done within the framework of the Passive Margin Exploration Laboratories (PAMELA) project, funded by TOTAL and IFREMER. IFREMER furthermore funded the contract of NS to study the meiofauna collected during the PAMELA-MOZ04 campaign. DC was supported by a predoctoral fellowship of the Complutense University of Madrid (CT27/16-CT28-16) and a short-term predoctoral fellowship also of the Complutense University of Madrid (EB14/19).

ACKNOWLEDGMENTS

We would like to thank all the participants and the staff of the R/V *L'Atalante* and *Pour quoi pas?* Vessel, Scampi team and all scientists and students who participated in the PAMELA MOZ1 and MOZ4 cruises, specially to Dr. Karine Olu, chief of the mission, and Lara Macheriotou for processing the cores on board. Moreover, we are grateful to the Ghent meiofauna laboratory for the meiofauna processing and Dr. Lucie Pastor and Christophe Brandily (IFREMER) for the geochemical analyses and advises in the treatment of geo-chemical data. We would also like to thank Dr. Martin V. Sorensen and Dr. Matteo Dal Zotto for their suggestions and comments that kindly improved the present article.

SUPPLEMENTARY MATERIAL

The Supplementary Material for this article can be found online at: https://www.frontiersin.org/articles/10.3389/fmars.2020.00665/full#supplementary-material

REFERENCES

Adrianov, A. V., and Maiorova, A. S. (2015). *Pycnophyes abyssorum* sp. n. (Kinorhyncha: Homalorhagida), the deepest kinorhynch species described so far. *Deep Sea Res. II Top. Stud. Oceanogr.* 111, 49–59. doi: 10.1016/j.dsr2.2014.08.009

Adrianov, A. V., and Maiorova, A. S. (2016). *Condyloderes kurilensis* sp. nov. (Kinorhyncha: Cyclorhagida)—a new deep water species from the abyssal plain near the Kuril-Kamchatka Trench. *Russ. J. Mar. Biol.* 42, 11–19. doi: 10.1134/S1063074016010028

Adrianov, A. V., and Maiorova, A. S. (2018a). *Meristoderes okhotensis* sp. nov. – The first deepwater representative of kinorhynchs in the Sea of Okhotsk (Kinorhyncha: Cyclorhagida). *Deep Sea Res. II Top. Stud. Oceanogr.* 154, 99–105. doi: 10.1016/j.dsr2.2017.10.011

Adrianov, A. V., and Maiorova, A. S. (2018b). *Parasemnoderes intermedius* gen. n., sp. n.—the First Abyssal Representative of the Family Semnoderidae (Kinorhyncha: Cyclorhagida). *Russ. J. Mar. Biol.* 44, 355–362. doi: 10.1134/S1063074018050024

Adrianov, A. V., and Malakhov, V. V. (1999). *Cephalorhyncha of the World Ocean*. Moscow: KMK Scientific Press.

Álvarez-Castillo, L., Cepeda, D., Pardos, F., Rivas, G., and Rocha-Olivares, Á (2020). *Echinoderes unispinosus* (Kinorhyncha: Cyclorhagida), a new record from deep-sea sediments in the Gulf of Mexico. *Zootaxa* 4821, 196–200.

Álvarez-Castillo, L., Hermoso-Salazar, M., Estradas-Romero, A., Prol-Ledesma, R. M., and Pardos, F. (2015). First records of *Kinorhyncha* from the Gulf of California: horizontal and vertical distribution of four genera in shallow basins with CO2 venting activity. *Cah. Biol. Mar.* 56, 271–281.

Bagarinao, T. (1992). Sulfide as an environmental factor and toxicant: tolerance and adaptations in aquatic organisms. *Aquat. Toxicol.* 24, 21–62. doi: 10.1016/0166-445X(92)90015-F

Cepeda, D., Álvarez-Castillo, L., Hermoso-Salazar, M., Sánchez, N., Gómez, S., and Pardos, F. (2019a). Four new species of Kinorhyncha from the Gulf of California, eastern Pacific Ocean. *Zool. Anz.* 282, 140–160. doi: 10.1016/j.jcz.2019.05.011

Cepeda, D., Sánchez, N., and Pardos, F. (2019b). First extensive account of the phylum Kinorhyncha from Haiti and the Dominican Republic (Caribbean Sea), with the description of four new species. *Mar. Biodivers.* 49, 2281–2309. doi: 10.1007/s12526-019-00963-x

Claparède, A. R. E. (1863). *Zur Kenntnis der Gattung Echinoderes Duj. Beobachtungen über Anatomie und Entwicklungsgeschichte wirbelloser Thiere an der Küste von Normandie angestellt*. Leipzig: Engelmann.

Colangelo, M. A., Bertasi, F., Dall'Olio, P., and Ceccherelli, V. H. (2001). "Meiofaunal biodiversity on hydrothermal seepage off Panarea (Aeolian Islands, Tyrrhenian Sea)," in *Mediterranean Ecosystems: Structures and Processes*, eds F. M. Faranda, L. Guglielmo, and G. Spezie (Berlin: Springer-Verlag), 353–359. doi: 10.1007/978-88-470-2105-1_46

Coull, B. C. (1985). Long-term variability of estuarine meiobenthos: an 11 year study. *Mar. Ecol. Prog. Ser.* 24, 205–218. doi: 10.3354/meps024205

Coull, B. C. (1988). "Ecology of the marine meiofauna," in *Introduction to the Study of Meiofauna*, eds R. P. Higgins and H. Thiel (Washington D.C: Smithsonian Institution Press), 18–38.

Dal Zotto, M., Santulli, A., Simonini, R., and Todaro, M. A. (2016). Organic enrichment effects on a marine meiofauna community, with focus on Kinorhyncha. *Zool. Anz.* 265, 127–140. doi: 10.1016/j.jcz.2016.03.013

Dando, P. R., Austen, M. C., Burke, R. A., Kendall, M. A., Kennicutt, M. C., Judd, A. G., et al. (1991). Ecology of a North Sea pockmark with an active methane seep. *Mar. Ecol. Prog. Ser.* 70, 49–63. doi: 10.3354/meps070049

Eakins, B. W., and Sharman, G. F. (2010). *Volumes of the World's Oceans from ETOPO1*. Boulder, CO: NOAA National Geophysical Data Center.

Fonselius, S. H. (1983). "Determination of hydrogen sulphide," in *Methods of Seawater Analysis*, eds K. Grasshoff, K. Kremling, and M. Ehrhardt (Weinheim: Verlag Chemie), 73–80.

Giere, O. (2009). *Meiobenthology. The Microscopic Motile Fauna of Aquatic Sediments*. Berlin: Springer.

Giovannelli, D., D'Errico, G., Fiorentino, F., Fattorini, D., Regoli, F., Angeletti, L., et al. (2016). Diversity and distribution of prokaryotes within a shallow-water pockmark field. *Front. Microbiol.* 7:941. doi: 10.3389/fmicb.2016.00941

Grzelak, K., and Sørensen, M. V. (2018). New species of Echinoderes (Kinorhyncha: Cyclorhagida) from Spitsbergen, with additional information about known Arctic species. *Mar. Biol. Res.* 14, 113–147. doi: 10.1080/17451000.2017.1367096

Grzelak, K., and Sørensen, M. V. (2019). Diversity and community structure of kinorhynchs around Svalbard: first insights into spatial patterns and environmental drivers. *Zool. Anz.* 282, 31–43. doi: 10.1016/j.jcz.2019.05.009

Guillon, E., Menot, L., Decker, C., Krylova, E., and Olu, K. (2017). The vesicomyd bivalve habitat at cold-seeps supports heterogeneous and dynamic macrofaunal assemblages. *Deep Sea Res. I Oceanogr. Res. Pap.* 120, 1–13. doi: 10.1016/j.dsr.2016.12.008

Heip, C. H. R., Vincx, M., and Vranken, G. (1985). The ecology of marine nematodes. *Oceanogr. Mar. Biol.* 23, 399–489.

Herranz, M., and Pardos, F. (2013). *Fissuroderes sorenseni* sp. nov. and *Meristoderes boylei* sp. nov.: first Atlantic recording of two rare kinorhynch genera, with new identification keys. *Zool. Anz.* 2013, 93–111. doi: 10.1016/j.jcz.2013.09.005

Herranz, M., Thormar, J., Benito, J., Sánchez, N., and Pardos, F. (2012). *Meristoderes* gen. nov., a new kinorhynch genus, with the description of two new species and their implications for echinoderid phylogeny (Kinorhyncha: Cyclorhagida, Echinoderidae). *Zool. Anz.* 251, 161–179. doi: 10.1016/j.jcz.2011.08.004

Higgins, R. P. (1969). Indian Ocean Kinorhyncha: 1. *Condyloderes* and Sphenoderes, new cyclorhagid genera. *Smith. Contr. Zool.* 14, 1–13. doi: 10.5479/si.00810282.14

Higgins, R. P. (1983). The Atlantic barrier reef ecosystem at Carrie Bow Cay, Belize, II. *Kinorhyncha. Smith. Contr. Mar. Sci.* 1, 1–131. doi: 10.5479/si.01960768.18.1

Hourdez, S., and Lallier, F. H. (2006). Adaptations to hypoxia in hydrothermal-vent and cold-seep invertebrates. *Rev. Environ. Sci. Biotechnol.* 6, 143–159. doi: 10.1007/s11157-006-9110-3

Hovland, M., and Judd, A. G. (1988). *Seabed Pockmarks and Seepages: Impact on Geology, Biology and Marine Environment*. London: Grahamand Trotman.

Janssen, A., Kaiser, S., Meißner, K., Brenke, N., Menot, L., and Arbizu, P. (2015). A reverse taxonomic approach to assess macrofaunal distribution patterns in abyssal Pacific polymetallic nodule fields. *PLoS One* 10:e0117790. doi: 10.1371/journal.pone.0117790

Jouet, G., and Deville, E. (2015). *PAMELA-MOZ04 cruise, R/V Pourquoi pas? Flotte océanographique française opérée par l'Ifremer*. Netherlands: EAGE.

Kennedy, B. R. C., Cantwell, K., Malik, M., Kelley, C., Potter, J., Elliott, K., et al. (2019). The unknown and the unexplored: insights into the Pacific deep-sea following NOAA CAPSTONE expeditions. *Front. Mar. Sci.* 6:480. doi: 10.3389/fmars.2019.00480

Kumar, A. (2017). "Foreword," in *Investigating Seafloors and Oceans, from Mud Volcanoes to Giant Squid*, ed. A. Joseph (Amsterdam: Elsevier), 9–26.

Landers, S. C., Basshman, R. D., Miller, J. A., Ingels, J., Sánchez, N., and Sørensen, M. V. (2020). Kinorhynch communities from Alabama coastal waters. *Mar. Biol. Res.* doi: 10.1080/17451000.2020.1789660

Landers, S. C., Sørensen, M. V., Beaton, K. R., Jones, C. M., Miller, J. M., and Stewart, P. M. (2018). Kinorhynch assemblages in the Gulf of Mexico continental shelf collected during a two-year survey. *J. Exp. Mar. Biol. Ecol.* 02, 81–90. doi: 10.1016/j.jembe.2017.05.013

Legendre, P., and Gallagher, E. D. (2001). Ecologically meaningful transformations for ordination of species data. *Oecology* 129, 271–280. doi: 10.1007/s004420100716

Levin, L. A. (2005). Ecology of cold seep sediments: interactions of fauna with flow, chemistry and microbes. *Oceanogr. Mar. Biol.* 43, 1–46. doi: 10.1201/9781420037449-3

Levin, L. A., and Sibuet, M. (2012). Understanding continental margin biodiversity: a new imperative. *Annu. Rev. Mar Sci.* 4, 79–112. doi: 10.1146/annurev-marine-120709-142714

Mirto, S., Gristina, M., Sinopoli, M., Maricchiolo, G., Genovese, L., Vizzini, S., et al. (2012). Meiofauna as an indicator for assessing the impact of fish farming at an exposed marine site. *Ecol. Indic.* 18, 468–476. doi: 10.1016/j.ecolind.2011.12.015

Mullineaux, L. S., Le Bris, N., Mills, S. W., Henri, P., Bayer, S. R., Secrist, R. G., et al. (2012). Detecting the influence of initial pioneers on succession at deep-sea vents. *PLoS One* 7:e50015. doi: 10.1371/journal.pone.0050015

Neuhaus, B. (2013). "Kinorhyncha (=Echinodera)," in *Handbook of Zoology. Gastrotricha, Cycloneuralia and Gnathifera, Volume 1: Nematomorpha,*

Priapulida, Kinorhyncha, Loricifera, ed. A. Schmidt-Rhaesa (Hamburg: De Gruyter), 181–350.

Neuhaus, B., and Blasche, T. (2006). Fissuroderes, a new genus of Kinorhyncha (Cyclorhagida) from the deep sea and continental shelf of New Zealand and from the continental shelf of Costa Rica. *Zool. Anz.* 245, 19–52. doi: 10.1016/j.jcz.2006.03.003

Neuhaus, B., and Sørensen, M. V. (2013). Populations of *Campyloderes* sp. (Kinorhyncha, Cyclorhagida): one global species with significant morphological variation? *Zool. Anz.* 252, 48–75. doi: 10.1016/j.jcz.2012.03.002

Oksanen, F. J., Blanchet, F. G., Friendly, M., Kindt, R., Legendre, P., McGlinn, D., et al. (2018). *vegan: Community Ecology Package. R Package Version 2.4-4*. Available online at: https://github.com/vegandevs/vegan (accessed October 02, 2019).

Oksanen, F. J., Blanchet, F. G., Kindt, R., Legendre, P., Minchin, P. R., O'Hara, R. B., et al. (2015). *vegan: Community Ecology Package. R Package Vegan, Version 2.2-1*. Available online at: https://github.com/vegandevs/vegan (accessed October 02, 2019).

Olu, K. (2014). *PAMELA-MOZ01 cruise, R/V L'Atalante. Flotte océanographique française opérée par l'Ifremer*. Netherlands: EAGE.

Pastor, L., Brandily, C., Schmidt, S., Miramontes, E., Péron, M., Apperé, D., et al. (2020). Modern sedimentation and geochemical imprints in sediments from the NW Madagascar margin. *Mar. Geol.* 426:106184. doi: 10.1016/j.margeo.2020.106184

Reinhard, W. (1881). Über Echinoderes und Desmoscolex der Umgebung von Odessa. *Zool. Anz.* 4, 588–592.

Ristova, P. P., Wenzhöfer, F., Ramette, A., Felden, J., and Boetius, A. (2015). Spatial scales of bacterial community diversity at cold seeps (eastern Mediterranean Sea). *ISME J.* 9, 1306–1318. doi: 10.1038/ismej.2014.217

Ritt, B., Pierre, C., Gauthier, O., Wenzhöfer, F., Boetius, A., and Sarrazin, J. (2011). Diversity and distribution of cold-seep fauna associated with different geological and environmental settings at mud volcanoes and pockmarks of the Nile deep-sea fan. *Mar. Biol.* 158, 1187–1210. doi: 10.1007/s00227-011-1679-6

Ritt, B., Sarrazin, J., Caprais, J. C., Noël, P., Gauthier, O., Pierre, C., et al. (2010). First insights into the structure and environmental setting of cold-seep communities in the Marmara Sea. *Deep Sea Res. I Oceanogr. Res. Pap.* 57, 1120–1136. doi: 10.1016/j.dsr.2010.05.011

Rouse, G. W., and Fauchald, K. (1997). Cladistics and polychaetes. *Zool. Scr.* 26, 139–204. doi: 10.1111/j.1463-6409.1997.tb00412.x

Sánchez, N., Pardos, F., and Martínez-Arbizu, P. (2019a). Deep-sea Kinorhyncha diversity of the polymetallic nodule fields at the clarion-clipperton fracture zone (CCZ). *Zool. Anz.* 282, 88–105. doi: 10.1016/j.jcz.2019.05.007

Sánchez, N., Pardos, F., and Sørensen, M. V. (2014a). A new kinorhynch genus, Mixtophyes (Kinorhyncha: Homalorhagida), from the Guinea Basin deep-sea, with new data on the family Neocentrophyidae. *Helgol. Mar. Res.* 68, 221–239. doi: 10.1007/s10152-014-0383-6

Sánchez, N., Pardos, F., and Sørensen, M. V. (2014b). Deep-sea Kinorhyncha: two new species from the Guinea Basin, with evaluation of an unusual male feature. *Org. Divers. Evol.* 14, 349–361. doi: 10.1007/s13127-014-0182-6

Sánchez, N., Sørensen, M. V., and Landers, S. C. (2019b). Pycnophyidae (Kinorhyncha: Allomalorhagida) from the Gulf of Mexico: *Fujuriphyes viserioni* sp. nov. and a re-description of *Leiocanthus langi* (Higgins, 1964), with notes on its intraspecific variation. *Mar. Biodivers.* 49, 1857–1875. doi: 10.1007/s12526-019-00947-x

Sánchez, N., and Yamasaki, H. (2016). Two new Pycnophyidae species (Kinorhyncha: Allomalorhagida) from Japan lacking ventral tubes in males. *Zool. Anz.* 265, 80–89. doi: 10.1016/j.jcz.2016.04.001

Sánchez, N., Yamasaki, H., Pardos, F., Sørensen, M. V., and Martínez, A. (2016). Morphology disentangles the systematics of a ubiquitous but elusive meiofaunal group (Kinorhyncha: Pycnophyidae). *Cladistics* 32, 479–505. doi: 10.1111/cla.12143

Sarradin, P. M., and Caprais, J. C. (1996). Analysis of dissolved gases by headspace sampling gas chromatography with column and detector switching. Preliminary results. *Anal. Commun.* 33, 371–373. doi: 10.1039/ac9963300371

Seeberg-Elverfeldt, J., Schlüter, M., Feseker, T., and Koelling, M. (2005). Rhizon sampling of pore waters near the sediment/water interface of aquatic systems. *Limnol. Oceanogr. Meth.* 3, 361–371. doi: 10.4319/lom.2005.3.361

Seitzinger, S. P., Mayorga, E., Bouwman, A. F., Kroeze, C., Beusen, A. H. W., Billen, G., et al. (2010). Global river nutrient export: a scenario analysis of past and future trends. *Glob. Biogeochem. Cycles* 24:GB0A08. doi: 10.1029/2009GB003587

Sibuet, M., and Olu, K. (1998). Biogeography, biodiversity and fluid dependence of deep-sea cold-seep communities at active and passive margins. *Deep Sea Res. II Top. Stud. Oceanogr.* 45, 517–567. doi: 10.1016/S0967-0645(97)00074-X

Somero, G. N., Childress, J. J., and Anderson, A. E. (1989). Transport, metabolism and detoxification of hydrogen sulphide in animals from sulphide-rich marine environments. *Aquat. Sci.* 1, 591–614.

Sørensen, M. V. (2008a). A new kinorhynch genus from the Antarctic deep sea and a new species of Cephalorhyncha from Hawaii (Kinorhyncha: Cyclorhagida: Echionoderidae). *Org. Divers. Evol.* 8, e1–e232. doi: 10.1016/j.ode.2007.11.003

Sørensen, M. V. (2008b). Phylogenetic analysis of the Echinoderidae (Kinorhyncha: Cyclorhagida). *Org. Divers. Evol.* 8, 233–246. doi: 10.1016/j.ode.2007.11.002

Sørensen, M. V., Dal Zotto, M., Rho, H. S., Herranz, M., Sánchez, N., Pardos, F., et al. (2015). Phylogeny of Kinorhyncha based on morphology and two molecular loci. *PLoS One* 10:e0133440. doi: 10.1371/journal.pone.0133440

Sørensen, M. V., and Grzelak, K. (2018). New mud dragons from Svalbard: three new species of Cristaphyes and the first Arctic species of *Pycnophyes* (Kinorhyncha: Allomalorhagida: Pycnophyidae). *PeerJ* 6:e5653. doi: 10.7717/peerj.5653

Sørensen, M. V., Rohal, M., and Thistle, D. (2018). Deep-sea Echinoderidae (Kinorhyncha: Cyclorhagida) from the Northwest Pacific. *Eur. J. Taxon.* 456, 1–75. doi: 10.5852/ejt.2018.456

Sørensen, M. V., Thistle, D., and Landers, S. C. (2019). North American *Condyloderes* (Kinorhyncha: Cyclorhagida: Kentrorhagata): female dimorphism suggests moulting among adult *Condyloderes*. *Zool. Anz.* 282, 232–251. doi: 10.1016/j.jcz.2019.05.015

Sun, J., Zhang, Y., Xu, T., Zhang, Y., Mu, H., Zhang, Y., et al. (2017). Adaptation to deep-sea chemosynthetic environments as revealed by mussel genomes. *Nat. Ecol. Evol.* 1:0121. doi: 10.1038/s41559-017-0121

Sutherland, T. F., Levings, C. D., Petersen, S. A., Poon, P., and Piercey, B. (2007). The use of meiofauna as an indicator of benthic organic enrichment associated with salmonid aquaculture. *Mar. Poll. Bull.* 54, 1249–1261. doi: 10.1016/j.marpolbul.2007.03.024

Van Gaever, S., Olu, K., Derycke, S., and Vanreusel, A. (2009). Metazoan meiofaunal communities at cold-seeps along the Norwegian margin: influence of habitat heterogeneity and evidence for connection with shallow-water habitats. *Deep Sea Res. I Oceanogr. Res. Pap.* 56, 772–785. doi: 10.1016/j.dsr.2008.12.015

Vanreusel, A., De Groote, A., Gollner, S., and Bright, M. (2010). Ecology and biogeography of free-living nematodes associated with chemosynthetic environments in the deep-sea: a review. *PLoS One* 5:e12449. doi: 10.1371/journal.pone.0012449

Yamasaki, H. (2016). Ryuguderes iejimaensis, a new genus and species of Campyloderidae (Xenosomata: Cyclorhagida: Kinorhyncha) from a submarine cave in the Ryukyu Islands, Japan. *Zool. Anz.* 265, 69–79. doi: 10.1016/j.jcz.2016.02.003

Yamasaki, H., Grzelak, K., Sørensen, M. V., Neuhaus, B., and George, K. H. (2018a). Echinoderes pterus sp. n. showing a geographically and bathymetrically wide distribution pattern on seamounts and on the deep-sea floor in the Arctic Ocean, Atlantic Ocean, and the Mediterranean Sea (Kinorhyncha, Cyclorhagida). *ZooKeys* 771, 15–40. doi: 10.3897/zookeys.771.25534

Yamasaki, H., Neuhaus, B., and George, K. H. (2018b). New species of Echinoderes (Kinorhyncha: Cyclorhagida) from Mediterranean seamounts and from the deep-sea floor in the North-eastern Atlantic Ocean, including notes of two undescribed species. *Zootaxa* 4387, 541–556. doi: 10.11646/zootaxa.4387.3.8

Yamasaki, H., Neuhaus, B., and George, K. H. (2018c). Three new species of Echinoderidae (Kinorhyncha: Cyclorhagida) from two seamounts and the adjacent deep-sea floor in the Northeast Atlantic Ocean. *Cah. Biol. Mar.* 59, 79–106. doi: 10.21411/CBM.A.124081A9

Yamasaki, H., Neuhaus, B., and George, K. H. (2019). Echinoderid mud dragons (Cyclorhagida: Kinorhyncha) from Senghor Seamount (NE Atlantic Ocean) including general discussion of faunistic characters and distribution patterns of seamount kinorhynchs. *Zool. Anz.* 282, 64–87. doi: 10.1016/j.jcz.2019.05.018

Zelinka, K. (1894). Über die Organisation von *Echinoderes*. *Verh. Dtsch. Zool. Ges.* 4, 46–49.

Zelinka, K. (1896). Demonstration der Tafeln der Echinoderes-Monographie. *Verh. Dtsch. Zool. Ges.* 6, 197–199.

Zelinka, K. (1913) Die Echinoderen der Deutschen Südpolar-Expedition 1901–1903. *Deutsche Südpolar Expedition XIV Zoologie* 6, 419–437.

Zelinka, K. (1928). *Monographie der Echinodera*. Leipzig: Engelmann.

Zeppilli, D., Canals, M., Danovaro, R., and Gambi, C. (2012). Meiofauna abundance of westerm Mediterranean Sea seep sediments. *PANGAEA*. doi: 10.1594/PANGAEA.803358

Zeppilli, D., and Danovaro, R. (2009). Meiofaunal diversity and assemblage structure in a shallow-water hydrothermal vent in the Pacific Ocean. *Aquat. Biol.* 5, 75–84. doi: 10.3354/ab00140

Zeppilli, D., Leduc, D., Fontanier, C., Fontaneto, D., Fuchs, S., Gooday, A. J., et al. (2018). Characteristics of meiofauna in extreme marine ecosystems: a review. *Mar. Biodivers.* 48, 35–71. doi: 10.1007/s12526-017-0815-z

Conflict of Interest: The authors declare that the research was conducted in the absence of any commercial or financial relationships that could be construed as a potential conflict of interest.

Copyright © 2020 Cepeda, Pardos, Zeppilli and Sánchez. This is an open-access article distributed under the terms of the Creative Commons Attribution License (CC BY). The use, distribution or reproduction in other forums is permitted, provided the original author(s) and the copyright owner(s) are credited and that the original publication in this journal is cited, in accordance with accepted academic practice. No use, distribution or reproduction is permitted which does not comply with these terms.